obtained with AM and PGE2 (data not shown). Stimulation of HUVECs with PGI2 and FSK dramatically enhanced accumulation of VE-cadherin at cell-cell contacts (Fig. 2B).

The maturation of AJ requires homophilic binding of intercellular VE-cadherins and tight anchoring to the actin cytoskeleton via the cytoplasmic region through catenins. VE-cadherin anchored to the actin cytoskeleton is detected in detergent-insoluble fractions of cell lysates (26). We found an increase in VE-cadherin in the Triton X-100-insoluble fraction after stimulation with PGI2 or FSK (Fig. 2C). These results suggest that cAMP-elevating GPCR agonists potentiate AJ formation, which results in a cAMP-induced decrease in permeability.

cAMP promotes VE-cadherin-dependent endothelial cell adhesion. VE-cadherin is required for AJ formation (9). To test the involvement of a homophilic interaction of VE-cadherin in cAMP-enhanced AJ formation, we directly examined VE-cadherin-mediated cell adhesion. To mimic the VE-cadherin-dependent cell adhesion, we used VEC-Fc chimeric protein, which consisted of the extracellular domain of VE-cadherin fused to the Fc portion of immunoglobulin. HUVECs were plated onto VEC-Fc-coated dishes and time-lapse imaged. Cells attached within 5 min to the VEC-Fc-coated dish, subsequently spread, and exhibited a typical fried-egg morphology characterized by a large circular lamellipodium (Fig. 3A). No cells attached to the Fc-coated dish (Fig. 3B and C). Since cadherin-dependent cell adhesion requires Ca^{2+}, we examined the effect of Ca^{2+} chelation on cell adhesion to VEC-Fc-coated dishes. Cell adhesion to VEC-Fc-coated dishes was completely abolished by chelating extracellular Ca^{2+}, although cell attachment to the collagen-coated dish was unaffected (Fig. 3C and D). Basal and FSK-augmented cell adhesion to VEC-Fc-coated dishes was inhibited by EGTA (Fig. 3C). Both HUVECs and HAECs expressing VE-cadherin adhered to the VEC-Fc-coated dish (Fig. 3E). In clear contrast, HeLa and HEK293 cells, which express N-cadherin, but not VE-cadherin (20, 42), did not adhere to the VEC-Fc-coated dish, although these cells could attach to the collagen-coated dish (Fig. 3E; data not shown). Collectively, these results indicate that endothelial cell adhesion to the VEC-Fc-coated dish depends upon the homophilic ligation of VE-cadherin.

We proceeded to investigate the effect of cAMP-elevating GPCR agonists on VE-cadherin-mediated cell adhesion. The adhesion of HUVECs plated in the presence of PGI2 or FSK was evaluated by the alkaline phosphatase activity of remaining cells after washing. PGI2 enhanced adhesion of HUVECs to the VEC-Fc-coated dish in a concentration-dependent manner (Fig. 4A) and in a time-dependent manner (Fig. 4B). In a time course analysis, we noticed that enhanced adhesion was observed 7 min after the plating (Fig. 4B). Other cAMP-elevating GPCR agonists, including AM, Iso, and PGE2, potentiated VE-cadherin-dependent cell adhesion (Fig. 4C). In addition, similarly enhanced cell adhesion to the VEC-Fc-coated dish was also observed in the cells treated with cAMP-elevating drugs such as IBMX, dbcAMP, and FSK (Fig. 4F). Like PGI2, the effect of FSK on cell adhesion to the VEC-Fc-coated dish was concentration dependent and time dependent (Fig. 4D and E). This cAMP-induced cell adhesion to the VEC-Fc-coated dish depends on the enhanced homophilic ligation of VE-cadherin because FSK did not augment endothelial adhe-

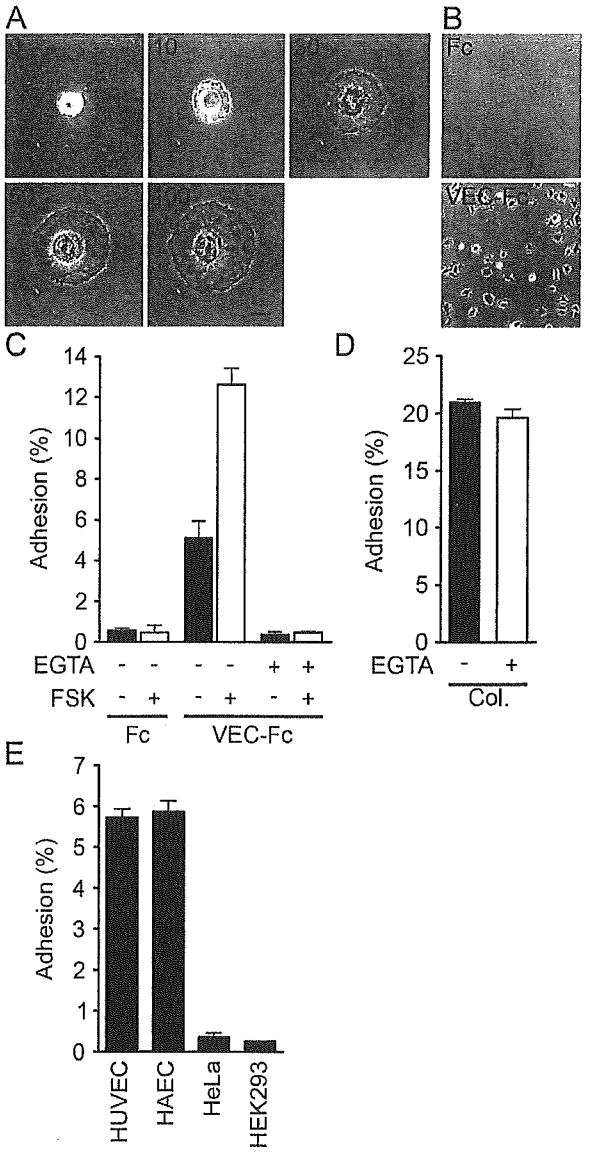

FIG. 3. Endothelial cells adhere to a VEC-Fc-coated dish through homophilic ligation of VE-cadherin. (A) HUVECs were plated onto the VEC-Fc-coated dish and time-lapse imaged at the time points (in minutes) indicated on the panels. Bar, 20 μM. (B) HUVECs were plated on the Fc-coated dish (top panel) or the VEC-Fc-coated dish (bottom panel) for 1 h and phase-contrast imaged after removal of nonadherent cells by washing with PBS-Ca/Mg. (C) HUVECs were plated onto either an Fc- or VEC-Fc-coated dish in the absence (−) or presence (+) of 5 mM EGTA and 10 μM FSK for 7 min. Cell adhesion was quantified as described in Materials and Methods. (D) Adhesion of HUVECs to a collagen-coated dish in the presence or absence of 5 mM EGTA was analyzed by a method similar to that described for panel C. (E) Adhesion of HUVECs, HAECs, and HeLa and HEK293 cells to the VEC-Fc-coated dish was examined as described in the legend for panel C. Cells adhering to the dishes of total input cells (percentage) is expressed as the mean ± standard deviation by measuring alkaline phosphatase activity of adherent cells divided by that of total input cells. Representative results from three independent experiments were shown in all panels.

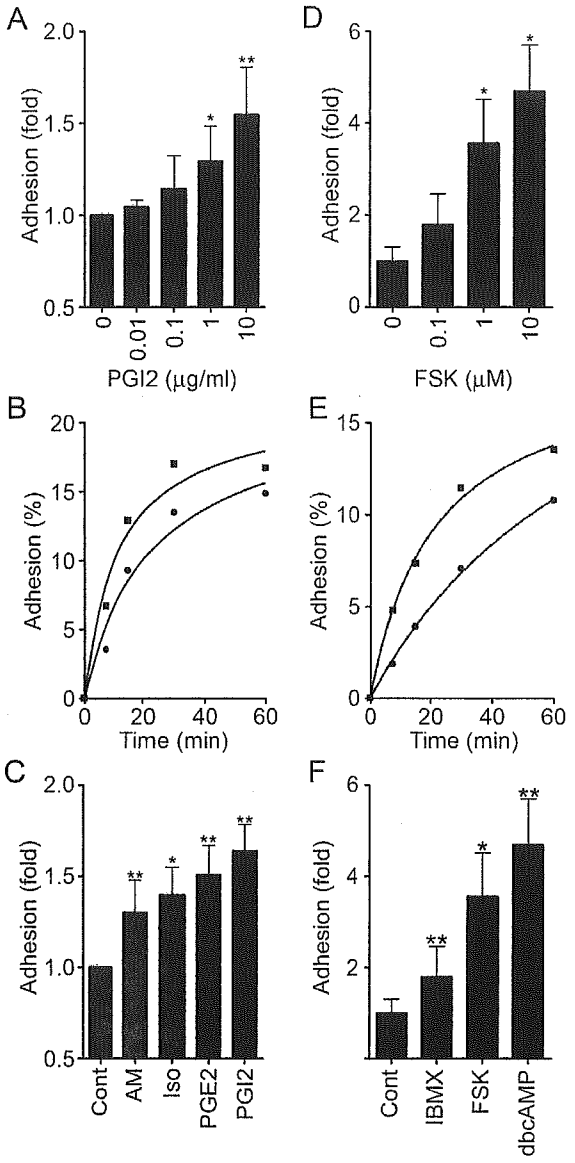

FIG. 4. cAMP potentiates VE-cadherin-dependent cell adhesion. (A) HUVECs were plated onto a VEC-Fc-coated dish in the presence of PGI2 at the concentrations indicated at the bottom for 7 min. Cell adhesion was quantified as described in Materials and Methods. Mean adhesion activity ± standard deviation is expressed as the increase compared with that observed in unstimulated cells. (B) HUVECs were plated onto the VEC-Fc-coated dish in the absence (circle) or presence (square) of 10-μg/ml PGI2 for the time indicated at the bottom. The percent adhesion was calculated by measuring the alkaline phosphatase activity of adherent cells divided by that of total input cells. (C) HUVECs stimulated with cAMP-elevating ligands similar to that described in the legend to panel A were assessed for adhesion activity. The concentration of stimulants was the same as described in the legend to Fig. 1A. (D) The effect of FSK on cell adhesion was analyzed by a method similar to that described for panel A, except that cells were preincubated for 10 min before plating. (E) The effect of 10 μM FSK on time-dependent adhesion was analyzed as described in the legend to panel B, except that cells were preincubated for 10 min before plating. (F) HUVECs stimulated with the reagent indicated at the same concentration used as described in the legend to Fig. 1A were analyzed for cell adhesion by a method similar to that described for panel D. Data are expressed as means ± standard deviations of the results from three independent experiments in panels A, C, D, and F. Representative results from three independent experiments were shown in panels B and E. A significant difference from the control determined by Student's *t* test is indicated with a single asterisk ($P < 0.05$) or double asterisks ($P < 0.01$).

sion to the Fc-coated dish or attachment to the VEC-Fc-coated dish in the absence of extracellular Ca^{2+} (Fig. 3C). These results indicate that cAMP potentiates VE-cadherin-dependent cell adhesion.

cAMP augments endothelial barrier function in a PKA-independent manner. PKA is suggested to be involved in cAMP-enhanced endothelial barrier function (43). Thus, we investigated the involvement of PKA in the regulation of endothelial barrier integrity by PGI2 and FSK. Unexpectedly, PGI2- and FSK-induced reduction of endothelial permeability was insensitive to a specific PKA inhibitor, H89 (7) (Fig. 5A and B). The reduction of thrombin-increased permeability by FSK was also unaffected by H89 (Fig. 5C). Consistently, H89 did not affect VE-cadherin-mediated cell adhesion enhancement by PGI2 and FSK (Fig. 5D and E). To confirm that H89 worked in HUVECs, we examined FSK-induced phosphorylation of CREB, a direct PKA substrate (38). Phosphorylation of CREB upon FSK stimulation was significantly inhibited by H89, indicating the effectiveness of this inhibitor in HUVECs (Fig. 5F). Therefore, these results apparently suggest a novel PKA-independent signaling pathway involved in cAMP-induced endothelial barrier function.

cAMP induces Rap1 activation. Besides PKA, Epac (cAMP-GEF) was identified as a novel cAMP target and a Rap1-specific GEF (5, 21). We therefore hypothesized that cAMP-activated Epac-Rap1 signaling is involved in the enhancement of VE-cadherin-dependent cell adhesion and endothelial barrier function. To address this possibility, we tested whether cAMP-elevating GPCR agonists induce Rap1 activation in HUVECs. Rap1 activity was determined by a pull-down assay by using a GST fusion protein of Rap1-binding domain of RalGDS according to the Bos's method. Bio-ligands for cAMP-elevating GPCR activated Rap1 (Fig. 6A). PGI2 rapidly induced Rap1 activation, which peaked at 1 to 5 min after the stimulation and then declined to the basal level by 10 min (Fig. 6C). A second wave of Rap1 activation was also observed 15 to 45 min after the stimulation (Fig. 6C). PGI2-induced Rap1 activation occurred in a concentration-dependent manner (Fig. 6B), which was associated with enhancement of VE-cadherin-dependent cell adhesion (Fig. 4A). Similarly, dbcAMP, FSK, and IBMX activated Rap1 (Fig. 6D). FSK-induced Rap1 activation reached a maximal level 2 to 5 min after the stimulation, and the level was sustained for up to 15 to 30 min (Fig. 6E). Collectively, these findings indicate that cAMP induces Rap1 activation in endothelial cells.

Specific activation of Epac reduces endothelial permeability and enhances VE-cadherin-dependent cell adhesion. To test whether the activation of endogenous Epac is sufficient to reduce endothelial permeability and to induce VE-cadherin-dependent cell adhesion, we used a recently developed cAMP analog, 8-CPT-2′-O-Me-cAMP, which specifically activates Epac without affecting PKA activity (13). As expected, 8-CPT-2′-O-Me-cAMP induced Rap1 activation in HUVECs (Fig. 7A), indicating that Epac is expressed in endothelial cells.

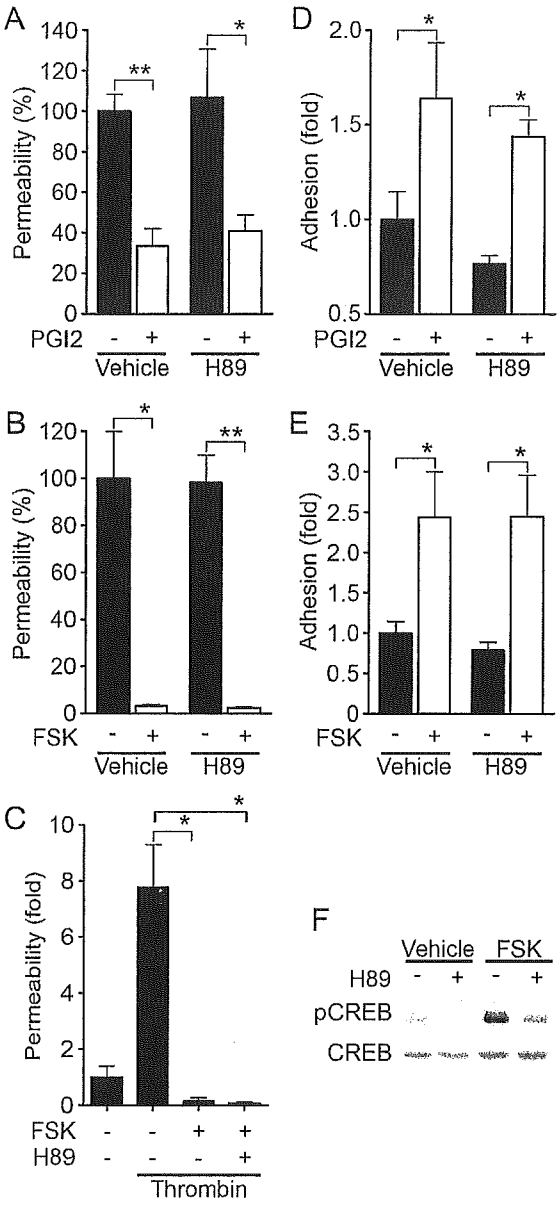

FIG. 5. cAMP-enhanced VE-cadherin-dependent cell adhesion and endothelial barrier function does not depend upon PKA. (A) Permeability across monolayer HUVECs grown on transwell filters were assessed by measuring FITC-labeled dextran as described in the legend to Fig. 1A. The effect of 10-μg/ml PGI2 on cell permeability without pretreatment (Vehicle) or with pretreatment with 5 μM H89, a specific PKA inhibitor, for 10 min is indicated as the percent permeability compared to that observed in untreated cells. +, present; −, absent. (B) The effect of 10 μM FSK on cell permeability without pretreatment (Vehicle) and with pretreatment with H89 was assessed similar to that described for panel A. (C) The effect of pretreatment of HUVECs with 5 μM H89 on FSK-induced reduction of 2-U/ml thrombin-induced permeability was analyzed. Permeability indicates the increase relative to that observed in untreated cells. (D) HUVECs untreated or pretreated with H89 for 10 min prior to stimulation with 10-μg/ml PGI2 were analyzed for cell adhesion as described in the legend to Fig. 4A. (E) HUVECs untreated or pretreated with H89 for 10 min prior to stimulation with 10 μM FSK were analyzed for cell adhesion as described in the legend to Fig. 4D. For panels A to E, data are expressed as means ± standard deviations of the results from triplicate samples. Similar results were obtained in at least three independent experiments. Significant differences between two groups determined by Student's *t* test are indicated by a single asterisk ($P < 0.05$) or double asterisks ($P < 0.01$). (F) HUVECs serum starved in 1% BSA-containing medium 199 for 6 h, followed by pretreatment with (+) or without (−) 5 μM H89 for 10 min, were stimulated with vehicle and 10 μM FSK for 10 min. Phosphorylation of CREB was assessed by Western blot analysis with anti-CREB (CREB) and anti-phospho-CREB-specific (pCREB) antibodies.

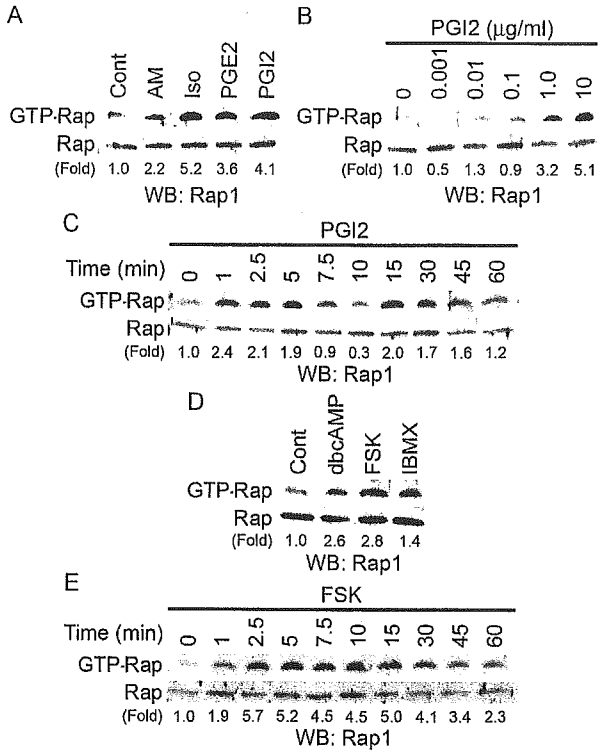

FIG. 6. cAMP induces Rap1 activation. (A) Serum-starved HUVECs kept in medium 199 containing 1% BSA overnight were stimulated with cAMP-elevating agonists for 2.5 min as indicated at the top and at the concentrations described in the legend to Fig. 1A. GTP-bound Rap1 was detected by pull-down assay as described in Materials and Methods. Activation indicates the ratio of the poststimulation GTP-Rap1 intensity of total Rap1 intensity to the prestimulation GTP-Rap1 intensity of total Rap1 intensity. (B) Rap1 activation was analyzed by detecting GTP-bound Rap1 with lysates from HUVECs stimulated with PGI2 for 2.5 min at the different concentrations indicated at the top. (C) Rap1 activation was analyzed by detecting GTP-bound Rap1 with lysates from cells stimulated with 10-μg/ml PGI2 for the time period indicated at the top. (D) Serum-starved HUVECs similar to those described in the legend to panel A were stimulated with the reagents indicated at the top for 10 min at the same concentrations described in the legend to Fig. 1A. Rap1 activation was assessed by a method similar to that described for panel A. (E) The effect of 10 μM FSK on time-dependent Rap1 activity was examined as described for panel C. Representative results from at least three independent experiments are shown for all panels.

8-CPT-2′-O-Me-cAMP dramatically reduced basal endothelial permeability, as did FSK and dbcAMP (Fig. 7B). Thrombin-induced permeability was also inhibited by 8-CPT-2′-O-Me-cAMP (Fig. 7C). Furthermore, we examined the effect of 8-CPT-2′-Me-cAMP on in vivo vascular permeability. VEGF-induced vascular permeability was completely blocked by coinjection of 8-CPT-2′-O-Me-cAMP (Fig. 7D). In addition, adhesion

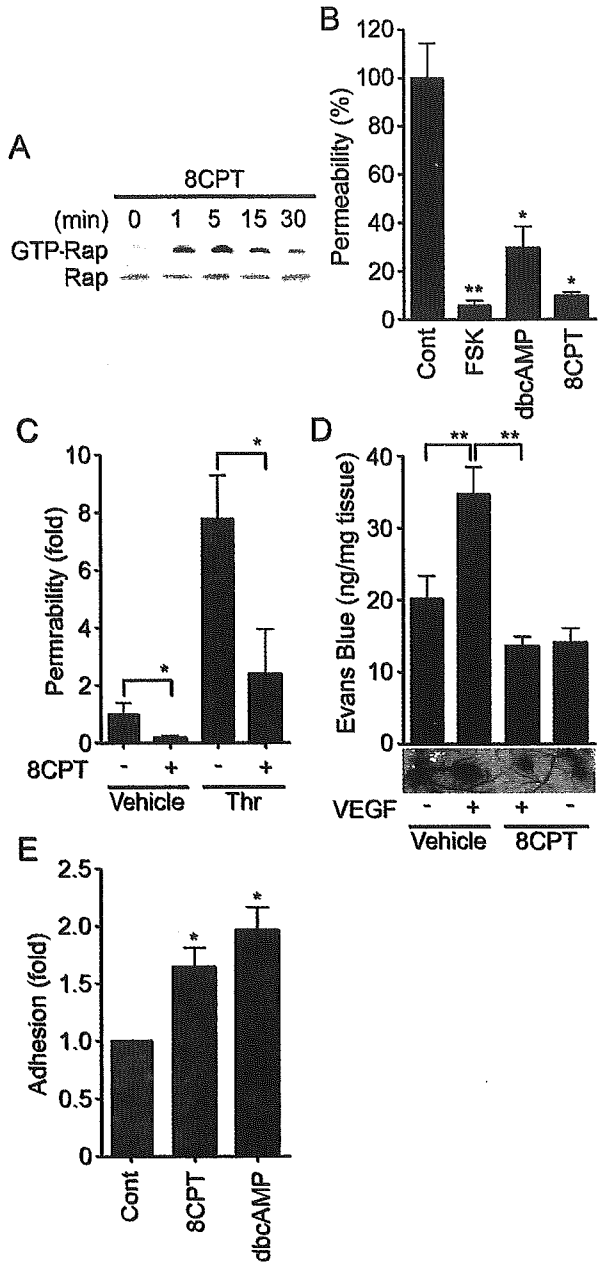

FIG. 7. Activation of Epac is sufficient to enhance VE-cadherin-dependent cell adhesion and endothelial barrier function. (A) Serum-starved HUVECs in medium 199 containing 1% BSA were stimulated with 0.2 mM 8-CPT-2′-O-Me-cAMP (8CPT) for the indicated time. Rap1 activity was determined as described in the legend to Fig. 6A. The result is a representative from three independent experiments. (B) Permeability of cells treated with the reagents as indicated on the bottom for 30 min was analyzed as described in the legend to Fig. 1A. (C) The effect of 0.2 mM 8CPT-2′-O-Me-cAMP on 2-U/ml thrombin-induced permeability was analyzed as described in the legend to Fig. 1B. (D) Effect of 8CPT-2′-O-Me-cAMP on VEGF-induced permeability was assessed by intradermal Miles assay as described in Materials and Methods. Amounts of extravasation of Evan blue in mouse dermal skin were measured 60 min after intradermal injection of vehicle and VEGF together with (+) or without (−) 8CPT. Mean leakage ± standard deviation of the results from 6 mice per group is expressed as nanograms of weight of extravasated Evans blue per milligram of weight of dermal skin. A photograph on the bottom shows leakage of Evans blue in dermal skin. (E) HUVEC adhesion to the VEC-Fc-coated dish in the presence of 0.2 mM 8CPT and 1 mM dbcAMP for 7 min was analyzed as described in the legend to Fig. 4F. In panels B, C, and E, data are expressed as means ± standard deviations of the results from triplicate samples. A significant difference from the control in panels B and E or between two groups in panels C and D was determined by Student's *t* test and indicated by a single asterisk ($P < 0.05$) or double asterisks ($P < 0.01$).

of HUVECs to the VEC-Fc-coated dish was significantly enhanced by 8-CPT-2′-O-Me-cAMP (Fig. 7E). Hence, Epac activation is sufficient to enhance VE-cadherin-dependent cell adhesion and to augment endothelial barrier function in vitro and in vivo.

Rap1 activation is essential for VE-cadherin-dependent cell adhesion and endothelial barrier function. We next proceeded to investigate the role of Rap1 in VE-cadherin-dependent cell adhesion and endothelial barrier function. To examine the effect of Rap1 on cell permeability and VE-cadherin-mediated cell adhesion, we inactivated endogenous Rap1 by adenovirus-expressing Rap1GAPII (Ad-RapGAP), which specifically catalyzes the hydrolysis of GTP to GDP on Rap1 (30). As shown in Fig. 8A, endogenous Rap1 activity was almost completely suppressed by the expression of increasing amounts of Rap1GAPII in HUVECs. This Rap1 inactivation paralleled the increase in basal permeability (Fig. 8B) and the inhibition of cell adhesion to the VEC-Fc-coated dish (Fig. 8D). In contrast, a constitutively active Rap1, Rap1V12, reduced both basal and thrombin-increased cell permeability (Fig. 8C). VE-cadherin-mediated cell adhesion was also enhanced by Rap1V12 and EpacΔcAMP, a constitutively active mutant of Epac (Fig. 8D). Taken together, these results indicate that Rap1 activation is required for VE-cadherin-mediated cell adhesion and endothelial barrier function.

cAMP enhances VE-cadherin-dependent cell adhesion and endothelial barrier function by activating Rap1. To test the requirement for Rap1 in endothelial barrier enhancement by cAMP-elevating GPCR agonists, we infected HUVECs with Ad-RapGAP and examined the effect of inactivation of Rap1 on PGI2- and FSK-induced reduction of cell permeability. Although basal endothelial permeability was reduced by PGI2 and FSK (Fig. 9A and B), overexpression of Rap1GAPII increased not only basal but also PGI2- and FSK-reduced endothelial permeability, indicating the requirement of Rap1 activity for PGI2- and FSK-induced barrier enhancement. We also investigated the involvement of Rap1 in PGI2- and FSK-induced VE-cadherin-dependent cell adhesion. PGI2 and FSK augmented VE-cadherin-dependent cell adhesion of HUVECs infected with control adenovirus (Ad-LacZ); however, their effects were dramatically suppressed by overexpression of Rap1GAPII (Fig. 9C and D). These data demonstrate that cAMP enhances VE-cadherin-dependent cell adhesion and endothelial barrier functions by activating Rap1.

cAMP induces endothelial cortical actin rearrangement in a Rap1-dependent manner. Endothelial barrier function is largely dependent upon the actin cytoskeleton supporting junctional adhesion molecules (10). Thus, we examined the effect of cAMP on cortical actin polymerization and assembly of polymerized actin in a monolayer of endothelial cells. Cortactin, an actin-binding protein, is known to be implicated in cortical actin rearrangement (8) and suggested to regulate S1P-induced endothelial barrier enhancement (11). PGI2,

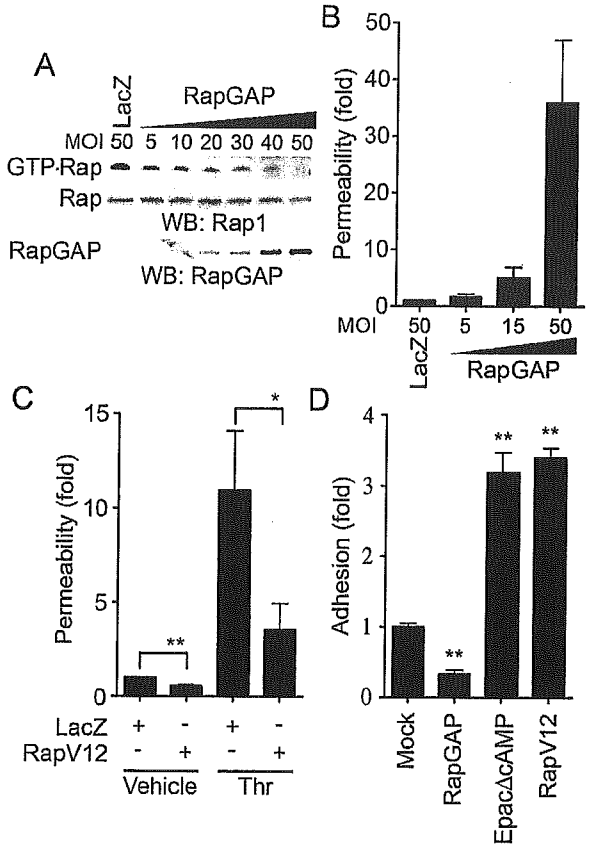

FIG. 8. Rap1 plays a critical role in VE-cadherin-dependent cell adhesion and endothelial barrier function. (A) Rap1 inactivation was assessed by detecting GTP-Rap1 in HUVECs infected with different MOI of adenovirus-expressing Rap1GAPII (RapGAP) as indicated at the top. An adenovirus-expressing LacZ at an MOI of 50 was used as a control. GTP-bound Rap1 (GTP-Rap) was detected by pull-down assay as described in Materials and Methods. Rap1 (Rap) and Rap1GAPII (RapGAP) expression were examined by Western blot analysis. (B) The permeability of FITC-dextran across HUVECs infected with adenovirus as indicated at the bottom was analyzed as described in Materials and Methods. Data are the means ± standard deviations of the results from three independent experiments and are expressed as increases relative to those of LacZ-infected cells. (C) Monolayer HUVECs infected with either an adenovirus-expressing LacZ or that expressing Rap1V12 at an MOI of 50 for 24 h were medium changed and cultured for another 24 h. The permeability of cells upon 2-U/ml thrombin stimulation (Thr) after starvation for 1 h was analyzed as described in the legend to Fig. 1B. Data are the means ± standard deviations of the results from five independent experiments and are expressed as inductions relative to those of untreated HUVECs infected with the LacZ-expressing virus. (D) HUVECs were transfected with either empty vector (Mock), plasmids expressing Rap1GAPII (RapGAP), EpacΔcAMP, or Rap1V12 together with the luciferase reporter construct. Transfected cells were plated on the VEC-Fc-coated dish and allowed to adhere for 15 min. Cell adhesion was analyzed as described in Materials and Methods. Data are expressed as increases compared to those of mock-transfected cells. The results indicate the means ± standard deviations of the results from triplicate samples. Similar results were obtained in three independent experiments. Significant differences between two groups in panel C or from the control in panel D are determined by Student's *t* test and are indicated by a single asterisk ($P < 0.05$) or double asterisks ($P < 0.01$).

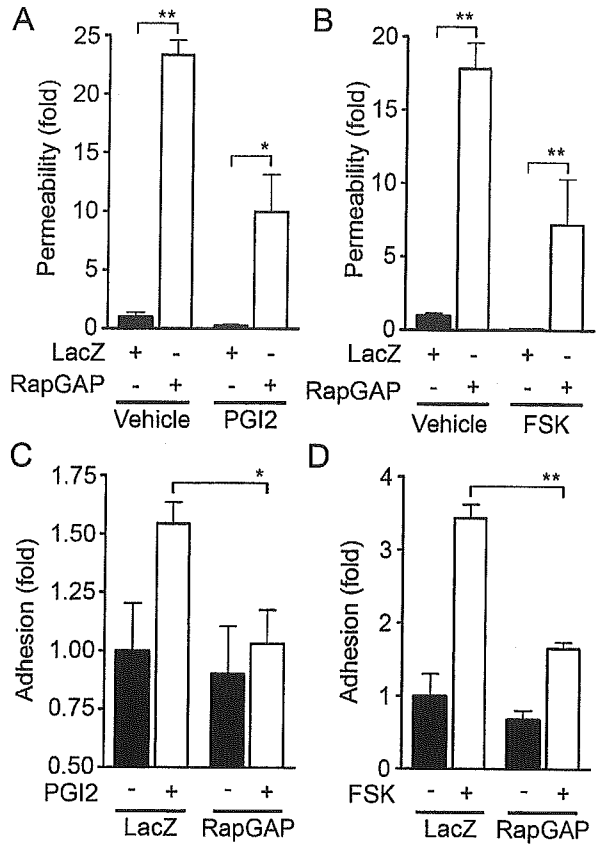

FIG. 9. Inactivation of Rap1 reduces PGI2- and FSK-induced barrier function and VE-cadherin-mediated cell adhesion. (A) Monolayer-cultured HUVECs grown on transwell filters were infected with either LacZ-expressing adenovirus (Ad-LacZ) or Rap1GAPII-expressing virus (Ad-RapGAP) at an MOI of 40 for 24 h. Medium was replaced with fresh medium after infection. Cells were cultured for an additional 24 h and treated with 10 μg of PGI2/ml for 30 min after serum starvation for 1 h. Permeability was analyzed as described in Materials and Methods. (B) The effect of 10 μM FSK on permeability in HUVECs infected with Ad-RapGAP was similarly analyzed. (C) HUVECs were infected with either Ad-LacZ or Ad-RapGAP at an MOI of 40 for 24 h. HUVECs resuspended in medium 199 with 0.5% BSA were plated onto VEC-Fc-coated dishes in the presence (+) or absence (−) of 10 μg of PGI2/ml for 7 min. Cell adhesion activity was quantified as described in the legend to Fig. 4A. (D) The effect of FSK on adhesion of HUVECs infected with Ad-RapGAP was analyzed similarly to that described for panel C. Resuspended HUVECs were preincubated with 10 μM FSK for 10 min before plating. Significant differences between two groups determined by Student's *t* test are indicated by a single asterisk ($P < 0.05$) or double asterisks ($P < 0.01$).

FSK, and 8-CPT-2′-O-Me-cAMP dramatically induced accumulation of polymerized actin and cortactin at cell-cell contacts (Fig. 10A). To explore the involvement of Rap1 in cAMP-mediated cortical actin rearrangement, an expression vector encoding Rap1GAPII was introduced into endothelial cells. FSK enhanced actin polymerization at cell-cell contacts in cells transfected with control vector encoding EGFP, whereas it did not in cells expressing Rap1GAPII (Fig. 10B). Cytochalasin D, an actin-depolymerizing agent, attenuated FSK-induced barrier enhancement (Fig. 10C) and inhibited FSK-induced VE-cadherin-dependent cell adhesion (Fig. 10D). These results suggest that the cortical actin rearrangement promoted by

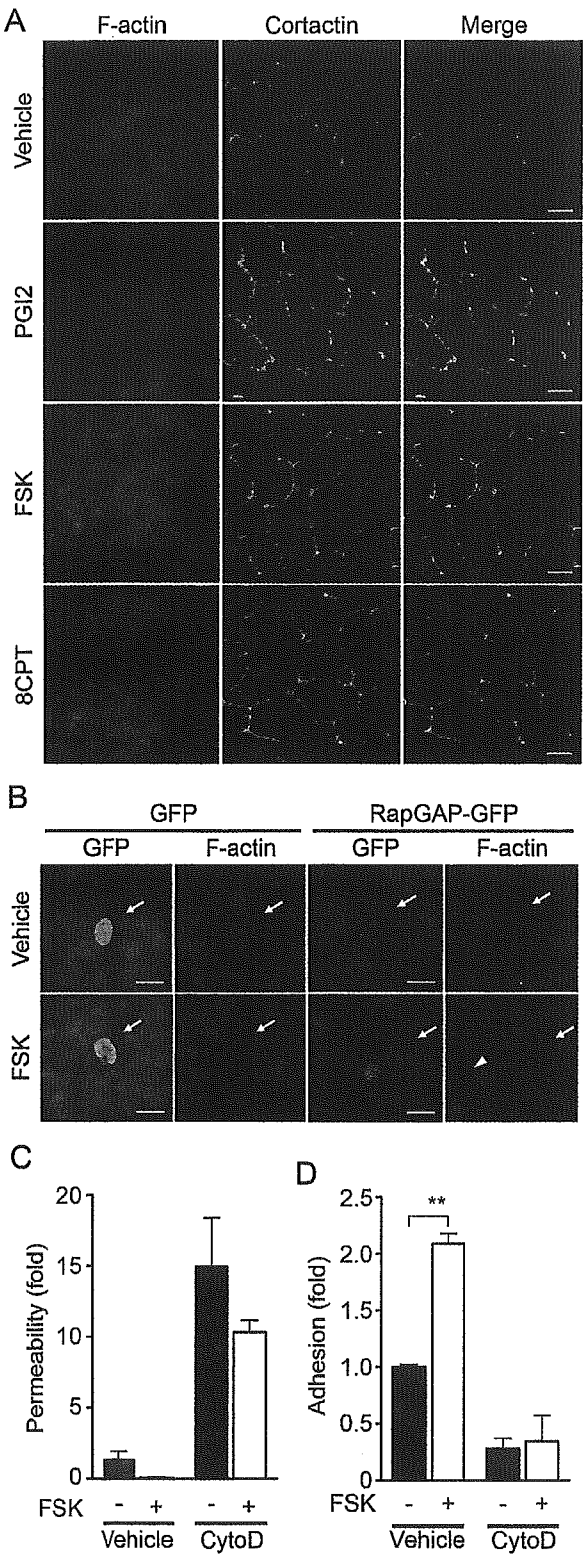

FIG. 10. cAMP induces cortical actin rearrangement in a Rap1-dependent manner. (A) Monolayer-cultured HUVECs starved in 0.5% BSA-containing medium 199 for 3 h were stimulated with vehicle (top row), 10-μg/ml PGI2 (second row), 10 μM FSK (third row), and 0.2 mM 8-CPT-2′-O-Me-cAMP (8CPT) (bottom row) for 30 min. Fixed and permeabilized cells were stained with rhodamine-phalloidin (left column) and with anti-cortactin (center column). Rhodamine images to detect F-actin (red) and Alexa 488 images for cortactin visualized by Alexa 488-labeled secondary antibody (green) were obtained through a confocal microscope (BX50WI). Right panels show the merged images of rhodamine and Alexa 488 images. Bars, 20 μm. (B) HUVECs transfected with an EGFP-expressing vector (left) and pCXN2-Rap1GAPII-IRES-EGFP (right) were serum starved in 0.5% BSA-containing medium 199 for 3 h and stimulated with vehicle (top panels) and 10 μM FSK (bottom panels). Cells were fixed, permeabilized, and stained with Rhodamine-phalloidin. EGFP images (green) and rhodamine images showing F-actin (red) were obtained similar to those in panel A. Arrows and arrowhead indicate transfected and untransfected cells, respectively. Bars, 20 μm. (C) Cell permeability of HUVECs pretreated with 2 μM cytochalasin D (CytoD) for 30 min followed by 10 μM FSK stimulation for 30 min was analyzed as described in the legend to Fig. 1A. −, absent; +, present. (D) The effect of pretreatment of 2 μM cytochalasin D (CytoD) on adhesion of HUVECs stimulated with FSK was analyzed as described in the legend to Fig. 5E. A significant difference between two groups determined by Student's *t* test is indicated by double asterisks ($P < 0.01$).

cAMP-Epac-Rap1 signaling may contribute to the potentiation of endothelial barrier function and VE-cadherin-dependent cell adhesion.

DISCUSSION

cAMP is a well-known intracellular signaling molecule that is capable of restoring diminished endothelial barrier function. Previous reports suggested that cAMP-induced barrier enhancement occurs through PKA (27, 39). In this study, however, we demonstrated a novel PKA-independent signaling pathway, the cAMP-Epac-Rap1 signaling pathway, involved in cAMP-induced barrier function based on the following observations. PGI2- and FSK-reduced endothelial permeability was insensitive to H89. A specific activator for Epac, 8-CPT-2′-O-Me-cAMP, reduced both basal and thrombin-increased permeability. Plasma leakage in response to VEGF was also inhibited by 8-CPT-2′-O-Me-cAMP in vivo. We found that the activation of Rap1 leads to decreased permeability. Not only all cAMP-elevating bio-ligands we tested but also FSK, db-cAMP, and IBMX activated Rap1. Consistently, cAMP-dependent Rap1 activation upon stimulation by these ligands involved Epac in the regulation of barrier function. A previous report showed that Rap1 is phosphorylated by PKA in neutrophils and platelets, although the function of phosphorylated Rap1 has not been elucidated (37). So far, Epac is known to regulate several biological functions including integrin-dependent cell adhesion, insulin secretion, and calcium release through ryanodine-sensitive Ca^{2+} channels (reviewed in reference 5). In addition to these Epac-mediated functions, we show, for the first time, that Epac-Rap1 signaling is important for regulation of endothelial barrier function.

AJ assembly contributes to the regulation of barrier function. Rap1 is involved in the formation and maintenance of AJ constituted by cadherin (23, 41). Recently, it has been reported that homophilic ligation of E-cadherin induced Rap1 activation, which may be responsible for maturation of AJ (20). Consistently, suppression of endogenous Rap1 inhibits formation of E-cadherin-dependent cell adhesion (36), suggesting the critical role of Rap1 in the establishment of cadherin-based cell-cell contacts. Here, we demonstrate that Rap1 also acts downstream of cAMP-Epac to potentiate VE-cadherin-depen-

dent cell adhesion, thereby improving barrier function. In addition to cAMP-elevating ligands, S1P, which enhances AJ formation and barrier function (18, 26), also activated Rap1 (our unpublished data). Thus, Rap1 may play a crucial role in barrier function induced by various types of barrier-improving factors.

Our data and previous studies show that cAMP protects thrombin-induced endothelial barrier dysfunction. cAMP does not limit the effect of thrombin on the initial loss of endothelial barrier (32). Instead, cAMP enhances the restoration of barrier function disrupted by thrombin. Recently, it was also reported that Cdc42 regulates the restoration of endothelial barrier function disrupted by thrombin (24). Thus, cAMP-Epac-Rap1 signaling may facilitate the formation of VE-cadherin-based cell-cell contacts, cooperatively or in parallel with Cdc42.

Rap1 enhances integrin-dependent cell adhesion in a variety of hematopoietic cells by modulating the affinity and avidity of integrin (6, 22). Cell adhesion to VEC-Fc-coated dishes was augmented by Rap1 activation, suggesting that the homophilic binding of VE-cadherin is also likely ascribed to the affinity and avidity of VE-cadherin modulated by Rap1-triggered inside out signaling. Hogan et al. reported that Rap1 activity is required for the targeting of E-cadherin molecules into nascent cell-cell contact sites, which in turn leads to the maturation of E-cadherin-based cell-cell contacts (20). Thus, cAMP-Epac-Rap1 signaling may also regulate the recruitment of VE-cadherin into maturing cell-cell contacts. Since downstream signaling of Rap1 that increases homophilic binding of VE-cadherin has not yet been characterized, the effector of cAMP-Epac-Rap1 signaling will need to be identified.

The actin cytoskeleton is a critical determinant of vascular integrity (10). PGI2, FSK, and 8-CPT-2′-O-Me-cAMP induced cortical actin rearrangement in a Rap1-dependent manner. FSK-induced VE-cadherin-dependent cell adhesion was inhibited by cytochalasin D. Thus, Rap1 may promote VE-cadherin-dependent cell adhesion by inducing cortical actin rearrangement. AF-6 may act downstream of Rap1 to regulate the actin cytoskeleton, since it binds to GTP-bound Rap1 and the actin cytoskeleton regulator, profilin, and is localized at AJ (2). Consistently, Canoe, the drosophila homolog of AF-6, and Rap1 function in the same molecular pathway during embryonic dorsal closure, which requires cell-cell contacts (3). S1P promotes endothelial barrier function by inducing Rac-dependent cortical actin rearrangement. S1P also induces Rap1 activation (our unpublished data). A previous report indicates that Rac can function downstream of Rap1 in the processing of the amyloid precursor protein (28). Taken together, Rac may act downstream of Rap1 to induce cortical actin rearrangement.

In conclusion, we have demonstrated that the cAMP-Epac-Rap1 signaling pathway promotes VE-cadherin-mediated cell adhesion and consequently improves endothelial barrier function.

ACKNOWLEDGMENTS

We thank J. L. Bos and W. A. Muller for plasmids, M. Matsuda and S. Hattori for adenovirus, J. T. Pearson for critical reading, and M. Sone, K. Yamamoto, and N. Irisawa for technical assistance.

This work was supported by grants from the Ministry of Health, Labor, and Welfare of Japan, from the Promotion of Fundamental Studies in Health Science of the Organization for Pharmaceutical Safety and Research of Japan, from the Ministry of Education, Science, Sports, and Culture of Japan, from the Uehara Memorial Foundation, and from Senri Life Science Foundation.

REFERENCES

1. **Andriopoulou, P., P. Navarro, A. Zanetti, M. G. Lampugnani, and E. Dejana.** 1999. Histamine induces tyrosine phosphorylation of endothelial cell-to-cell adherens junctions. Arterioscler. Thromb. Vasc. Biol. **19:**2286–2297.
2. **Boettner, B., E. E. Govek, J. Cross, and L. Van Aelst.** 2000. The junctional multidomain protein AF-6 is a binding partner of the Rap1A GTPase and associates with the actin cytoskeletal regulator profilin. Proc. Natl. Acad. Sci. USA **97:**9064–9069.
3. **Boettner, B., P. Harjes, S. Ishimaru, M. Heke, H. Q. Fan, Y. Qin, L. Van Aelst, and U. Gaul.** 2003. The AF-6 homolog canoe acts as a Rap1 effector during dorsal closure of the Drosophila embryo. Genetics **165:**159–169.
4. **Bogatcheva, N. V., J. G. Garcia, and A. D. Verin.** 2002. Molecular mechanisms of thrombin-induced endothelial cell permeability. Biochemistry (Moscow) **67:**75–84.
5. **Bos, J. L.** 2003. Epac: a new cAMP target and new avenues in cAMP research. Nat. Rev. Mol. Cell Biol. **4:**733–738.
6. **Bos, J. L., J. de Rooij, and K. A. Reedquist.** 2001. Rap1 signalling: adhering to new models. Nat. Rev. Mol. Cell Biol. **2:**369–377.
7. **Chijiwa, T., A. Mishima, M. Hagiwara, M. Sano, K. Hayashi, T. Inoue, K. Naito, T. Toshioka, and H. Hidaka.** 1990. Inhibition of forskolin-induced neurite outgrowth and protein phosphorylation by a newly synthesized selective inhibitor of cyclic AMP-dependent protein kinase, N-[2-(p-bromocinnamylamino)ethyl]-5-isoquinolinesulfonamide (H-89), of PC12D pheochromocytoma cells. J. Biol. Chem. **265:**5267–5272.
8. **Daly, R. J.** 2004. Cortactin signalling and dynamic actin networks. Biochem. J. **382:**13–25. [Online.] doi:10.1042/BJ20040737.
9. **Dejana, E.** 2004. Endothelial cell-cell junctions: happy together. Nat. Rev. Mol. Cell Biol. **5:**261–270.
10. **Dudek, S. M., and J. G. Garcia.** 2001. Cytoskeletal regulation of pulmonary vascular permeability. J. Appl. Physiol. **91:**1487–1500.
11. **Dudek, S. M., J. R. Jacobson, E. T. Chiang, K. G. Birukov, P. Wang, X. Zhan, and J. G. Garcia.** 2004. Pulmonary endothelial cell barrier enhancement by sphingosine 1-phosphate: roles for cortactin and myosin light chain kinase. J. Biol. Chem. **279:**24692–24700.
12. **Endo, A., K. Nagashima, H. Kurose, S. Mochizuki, M. Matsuda, and N. Mochizuki.** 2002. Sphingosine 1-phosphate induces membrane ruffling and increases motility of human umbilical vein endothelial cells via vascular endothelial growth factor receptor and CrkII. J. Biol. Chem. **277:**23747–23754.
13. **Enserink, J. M., A. E. Christensen, J. de Rooij, M. van Triest, F. Schwede, H. G. Genieser, S. O. Doskeland, J. L. Blank, and J. L. Bos.** 2002. A novel Epac-specific cAMP analogue demonstrates independent regulation of Rap1 and ERK. Nat. Cell Biol. **4:**901–906.
14. **Esser, S., M. G. Lampugnani, M. Corada, E. Dejana, and W. Risau.** 1998. Vascular endothelial growth factor induces VE-cadherin tyrosine phosphorylation in endothelial cells. J. Cell Sci. **111**(Pt 13):1853–1865.
15. **Farmer, P. J., S. G. Bernier, A. Lepage, G. Guillemette, D. Regoli, and P. Sirois.** 2001. Permeability of endothelial monolayers to albumin is increased by bradykinin and inhibited by prostaglandins. Am. J. Physiol. Lung Cell. Mol. Physiol. **280:**L732–L738.
16. **Fukuhara, S., M. J. Marinissen, M. Chiariello, and J. S. Gutkind.** 2000. Signaling from G protein-coupled receptors to ERK5/Big MAPK 1 involves Galpha q and Galpha 12/13 families of heterotrimeric G proteins. Evidence for the existence of a novel Ras AND Rho-independent pathway. J. Biol. Chem. **275:**21730–21736.
17. **Gamble, J. R., J. Drew, L. Trezise, A. Underwood, M. Parsons, L. Kasminkas, J. Rudge, G. Yancopoulos, and M. A. Vadas.** 2000. Angiopoietin-1 is an antipermeability and anti-inflammatory agent in vitro and targets cell junctions. Circ. Res. **87:**603–607.
18. **Garcia, J. G., F. Liu, A. D. Verin, A. Birukova, M. A. Dechert, W. T. Gerthoffer, J. R. Bamberg, and D. English.** 2001. Sphingosine 1-phosphate promotes endothelial cell barrier integrity by Edg-dependent cytoskeletal rearrangement. J. Clin. Investig. **108:**689–701.
19. **Hippenstiel, S., M. Witzenrath, B. Schmeck, A. Hocke, M. Krisp, M. Krull, J. Seybold, W. Seeger, W. Rascher, H. Schutte, and N. Suttorp.** 2002. Adrenomedullin reduces endothelial hyperpermeability. Circ. Res. **91:**618–625.
20. **Hogan, C., N. Serpente, P. Cogram, C. R. Hosking, C. U. Bialucha, S. M. Feller, V. M. M. Braga, W. Birchmeier, and Y. Fujita.** 2004. Rap1 regulates the formation of E-cadherin-based cell-cell contacts. Mol. Cell. Biol. **24:**6690–6700.
21. **Kawasaki, H., G. M. Springett, N. Mochizuki, S. Toki, M. Nakaya, M. Matsuda, D. E. Housman, and A. M. Graybiel.** 1998. A family of cAMP-binding proteins that directly activate Rap1. Science **282:**2275–2279.
22. **Kinbara, K., L. E. Goldfinger, M. Hansen, F. L. Chou, and M. H. Ginsberg.**

2003. Ras GTPases: integrins' friends or foes? Nat. Rev. Mol. Cell Biol. **4**:767–776.
23. **Knox, A. L., and N. H. Brown.** 2002. Rap1 GTPase regulation of adherens junction positioning and cell adhesion. Science **295**:1285–1288.
24. **Kouklis, P., M. Konstantoulaki, S. Vogel, M. Broman, and A. B. Malik.** 2004. Cdc42 regulates the restoration of endothelial barrier function. Circ. Res. **94**:159–166.
25. **Langeler, E. G., and V. W. van Hinsbergh.** 1991. Norepinephrine and iloprost improve barrier function of human endothelial cell monolayers: role of cAMP. Am. J. Physiol. **260**:C1052–C1059.
26. **Lee, M. J., S. Thangada, K. P. Claffey, N. Ancellin, C. H. Liu, M. Kluk, M. Volpi, R. I. Sha'afi, and T. Hla.** 1999. Vascular endothelial cell adherens junction assembly and morphogenesis induced by sphingosine-1-phosphate. Cell **99**:301–312.
27. **Lum, H., H. A. Jaffe, I. T. Schulz, A. Masood, A. RayChaudhury, and R. D. Green.** 1999. Expression of PKA inhibitor (PKI) gene abolishes cAMP-mediated protection to endothelial barrier dysfunction. Am. J. Physiol. **277**: C580–C588.
28. **Maillet, M., S. J. Robert, M. Cacquevel, M. Gastineau, D. Vivien, J. Bertoglio, J. L. Zugaza, R. Fischmeister, and F. Lezoualc'h.** 2003. Crosstalk between Rap1 and Rac regulates secretion of sAPPalpha. Nat. Cell Biol. **5**:633–639.
29. **Miles, A. A., and E. M. Miles.** 1952. Vascular reactions to histamine, histamine-liberator and leukotaxine in the skin of guinea-pigs. J. Physiol. **118**: 228–257.
30. **Mochizuki, N., Y. Ohba, E. Kiyokawa, T. Kurata, T. Murakami, T. Ozaki, A. Kitabatake, K. Nagashima, and M. Matsuda.** 1999. Activation of the ERK/MAPK pathway by an isoform of rap1GAP associated with G alpha(i). Nature **400**:891–894.
31. **Mori, Y., T. Nishikimi, N. Kobayashi, H. Ono, K. Kangawa, and H. Matsuoka.** 2002. Long-term adrenomedullin infusion improves survival in malignant hypertensive rats. Hypertension **40**:107–113.
32. **Moy, A. B., J. E. Bodmer, K. Blackwell, S. Shasby, and D. M. Shasby.** 1998. cAMP protects endothelial barrier function independent of inhibiting MLC20-dependent tension development. Am. J. Physiol. **274**:L1024–L1029.
33. **Navarro, P., L. Ruco, and E. Dejana.** 1998. Differential localization of VE- and N-cadherins in human endothelial cells: VE-cadherin competes with N-cadherin for junctional localization. J. Cell Biol. **140**:1475–1484.
34. **Ohba, Y., K. Ikuta, A. Ogura, J. Matsuda, N. Mochizuki, K. Nagashima, K. Kurokawa, B. J. Mayer, K. Maki, J. Miyazaki, and M. Matsuda.** 2001. Requirement for C3G-dependent Rap1 activation for cell adhesion and embryogenesis. EMBO J. **20**:3333–3341.
35. **Parandoosh, Z., C. A. Bogowitz, and M. P. Nova.** 1998. A fluorometric assay for the measurement of endothelial cell density in vitro. In Vitro Cell. Dev. Biol. Anim. **34**:772–776.
36. **Price, L. S., A. Hajdo-Milasinovic, J. Zhao, F. J. Zwartkruis, J. G. Collard, and J. L. Bos.** 2004. Rap1 regulates E-cadherin-mediated cell-cell adhesion. J. Biol. Chem. **279**:35127–35132.
37. **Quilliam, L. A., H. Mueller, B. P. Bohl, V. Prossnitz, L. A. Sklar, C. J. Der, and G. M. Bokoch.** 1991. Rap1A is a substrate for cyclic AMP-dependent protein kinase in human neutrophils. J. Immunol. **147**:1628–1635.
38. **Shaywitz, A. J., and M. E. Greenberg.** 1999. CREB: a stimulus-induced transcription factor activated by a diverse array of extracellular signals. Annu. Rev. Biochem. **68**:821–861.
39. **Stelzner, T. J., J. V. Weil, and R. F. O'Brien.** 1989. Role of cyclic adenosine monophosphate in the induction of endothelial barrier properties. J. Cell. Physiol. **139**:157–166.
40. **Ukropec, J. A., M. K. Hollinger, S. M. Salva, and M. J. Woolkalis.** 2000. SHP2 association with VE-cadherin complexes in human endothelial cells is regulated by thrombin. J. Biol. Chem. **275**:5983–5986.
41. **Yajnik, V., C. Paulding, R. Sordella, A. I. McClatchey, M. Saito, D. C. Wahrer, P. Reynolds, D. W. Bell, R. Lake, S. van den Heuvel, J. Settleman, and D. A. Haber.** 2003. DOCK4, a GTPase activator, is disrupted during tumorigenesis. Cell **112**:673–684.
42. **Yano, H., Y. Mazaki, K. Kurokawa, S. K. Hanks, M. Matsuda, and H. Sabe.** 2004. Roles played by a subset of integrin signaling molecules in cadherin-based cell-cell adhesion. J. Cell Biol. **166**:283–295.
43. **Yuan, S. Y.** 2002. Protein kinase signaling in the modulation of microvascular permeability. Vascul. Pharmacol. **39**:213–223.

Characterization and gene transfer in mesenchymal stem cells derived from human umbilical-cord blood

FEI-ZHOU LU, MASAYUKI FUJINO, YUSUKE KITAZAWA, TARO UYAMA, YUKO HARA, NAOKO FUNESHIMA, JIAN-YUAN JIANG, AKIHIRO UMEZAWA, XIAO-KANG LI

TOKYO, JAPAN, AND SHANGHAI, CHINA

It has been shown that the stromal-cell population found in bone marrow can be expanded and differentiated into cells with the phenotypes of bone, cartilage, muscle, neural, and fat cells. However, whether mesenchymal stem cells (MSCs) are present in human umbilical-cord blood (UCB) has been the subject of ongoing debate. In this study, we report on a population of fibroblastlike cells derived from the mononuclear fraction of human UCB with osteogenic and adipogenic potential, as well as the presence of a subset of cells that have been maintained in continuous culture for more than 6 months. These cells were found to express CD29, CD44, CD90, CD95, CD105, CD166, and MHC class , but not CD14, CD34, CD40, CD45, CD80, CD86, CD117, CD152, or MHC class II. We also compared gene expression after gene transfer using lenti- and adenoviral vectors carrying the green fluorescence protein to the MSCs derived from UCB because a reliable gene-delivery system is required to transfer target genes into MSCs, which have attracted attention as potential platforms for the systemic delivery of therapeutic genes. The lentiviral vectors can transduce these cells more efficiently than can adenoviral vectors, and we maintained transgene expression for at least 5 weeks. This is the first report showing that UCB-derived MSCs can express exogenous genes by way of a lentivirus vector. These results demonstrate that human UCB is a source of mesenchymal progenitors and may be used in cell transplantation and a wide range of gene-therapy treatments. (J Lab Clin Med 2005;146:271-278)

Abbreviations: adeno-GFP = recombinant adenovirus expressing the green fluorescent protein gene Ax1CAGFP; BBS = BBS 50 mmol/L BES, 280 mmol/L NaCl, 1.5 mmol/L Na_2HPO_4; BM = bone marrow; DMEM = Dulbecco's modified Eagle medium; EDTA = ethylenediaminetetraacetic acid; FACS = fluorescence-activated cell sorting; FBS = fetal bovine serum; FITC = fluorescein isothiocyanate; GFP = green fluorescent protein; IU = infectious unit; lenti-GFP = lentivirus expressing the green fluorescent protein; MNC = mononuclear cell; MSC = mesenchymal stem cell; MSCGM = MSC growth medium; PBS = phosphate-buffered saline solution; TBST = Tris-buffered saline solution containing Tween-20; UCB = umbilical-cord blood

Human UCB has been reported to contain stem/progenitor cells at concentrations greater than or equal to those in bone marrow and adult peripheral blood.[1] UCB-cell transplantation for various blood diseases has recently been successful, with a lower incidence of graft-vs-host disease than that seen in many conventional treatments.[2] In these clinical applications, hematopoietic stem cells can differentiate to

From the Laboratory of Transplantation Immunology and the Department of Reproductive Biology and Pathology, National Research Institute for Child Health and Development, Tokyo, Japan; and the Department of Orthopedic Surgery, Huashan Hospital, Fudan University Medical School, Shanghai, China.

Supported by research grants from Japan Society for the Promotion of Science (PD-016); the Ministry of Education, Culture, Sports, Science, and Technology of Japan (grants-in-aid 14370367 and 13671250); a Grant for Organized Research Combination System; and a grant from the Natural Science Foundation of China (30371434).

Submitted for publication March 8, 2005; revision submitted May 27, 2005; accepted for publication July 4, 2005.

Reprint requests: Xiao-Kang Li, MD, PhD, Laboratory of Transplantation Immunology, National Research Institute for Child Health and Development, 2-10-1 Okura, Setagaya-ku, Tokyo 157-8535, Japan; e-mail: sri@nch.go.jp.

0022-2143/$ - see front matter

doi:10.1016/j.lab.2005.07.003

mature blood cells. It has been reported that CD34-positive cells, well-known stem-cell markers, have the capacity to differentiate into all blood-cell lineages.[3] After birth, UCB contains hematopoietic precursors, and it has become an important alternative source of hematopoietic stem cells for transplantation.

It is also widely accepted that MSCs, as well as hematopoietic stem cells, are present in BM. MSCs can differentiate into multiple lineages, including osteoblasts, chondrocytes, and adipocytes. This rare characteristic has resulted in speculation about the possibility of using BM-derived MSCs as a source of cell therapy for more than 5 years.[4–7] Recently human UCB cells were also reported to differentiate into a variety of cell types, such as hepatocytes and nerve and muscle cells, as well as bone, cartilage, and fat cells from the non-hematopoietic cell fraction that appears to comprise MSCs.[8–11] However, controversy continues as to whether human UCB contains MSCs.[12,13]

A reliable gene-delivery system is required to facilitate the transfer of target genes into MSCs that express therapeutic proteins, which cause tissues of mesenchymal origin to express gene products essential for tissue regeneration and repair. Previous studies involving nonviral vectors and replication-deficient recombinant adenovirus and adenovirus-associated viral vectors have demonstrated highly efficient gene transfer to MSCs.[14–19] Recently lentivirus has received considerable attention as a possible vector in the field of gene therapy. Although lentivirus is one of the subfamilies of retrovirus species, lentivirus vectors based on the human immunodeficiency virus genome have many advantages over retrovirus vectors, particularly their ability to transduce nondividing cells.[14–19] Furthermore, lentivirus vectors can integrate in the host genome and replace the natural glycoprotein envelope with G-glycoprotein of vesicular stomatitis, allowing the viral particles to infect a broad range of host-cells types. Therefore exogenous gene expression in target cells would be extended to much longer periods after gene transfer, regardless of the type of target organ, tissue, or cell. The lentivirus vector may therefore be considered ideal for long-term exogenous gene expression, especially for stem cells. Although the lentivirus vector has been proposed as a potential vector for gene transfer, and high-level gene expression of transduced stem cells of various types by viral and nonviral vectors has also been reported, transgene expression efficiency of MSCs derived from UCB infected with lentivirus vector has remained low.

In this study, we investigated the presence of multipotent progenitor cells in human UCB, similar to the cells derived from BM. We found that the mesenchymal progenitors in UCB do not express hematopoietic stem-cell or mononuclear-cell markers CD34, CD14, or CD45 and that they may be cultured and divided for periods of longer than 6 months. We also examined exogenous gene expression in UCB-derived MSCs, using lentivirus and adenovirus vectors because have been no reports as to whether lentivirus vector can transduce exogenous genes, yield enough gene expression to affect cell phenotype, or cause expression level in UCB-derived MSCs to persist. We hypothesize that lentiviral vectors facilitate extended periods of gene expression in MSCs. This is considered a useful characteristic for therapeutic applications because progenitor cells with human mesenchymal stem-cell characteristics may be used for both cell transplantation and gene therapy.

METHODS

Cell isolation and culture. Human UCB, 30 to 150 mL, was collected by way of venous puncture of the umbilical vein at the time of full-term delivery. Equal volumes of UCB and 6% hydroxyethyl starch (NIPRO, Osaka, Japan) were mixed in sterile centrifuge tubes and left to stand for 90 minutes. Red blood cells were allowed to settle by way of gravity. Nucleated cells were then obtained from the supernatant. After being washed twice with sterilized PBS, isolated UCB cells were primarily cultured in MSCGM (Cambrex Bio Science, Walkersville, Md). The cells were seeded at a density of 1×10^6 to 10^7 cells/cm^2, and the medium was changed after 5 days. Nonadherent cells were discarded. Thereafter, half of the medium was changed at weekly intervals. Cells were harvested with the use of 0.25% trypsin and 1 mmol/L EDTA when they reached 60% to 70% confluence, then replated at a density of 1000 to 2000 cells/cm^2. We assessed the structure of adherent cells with the us eof a phase-contrast microscope (Olympus, Tokyo, Japan). Cells were first harvested by means of cytospin centrifugation and then stained with May-Giemsa stain (Wako Pure Chemical Industries, Osaka, Japan). This research was carried out in accordance with the principles of the Declaration of Helsinki and under the approval of the ethical-review board of the National Center for Child Health and Development.

FACS analysis. We trypsinized the cells and then incubated them with fluorochrome-conjugated antibody, on ice, in the dark, for 20 minutes; rinsed them twice with cold PBS; and fixed them with cold, freshly prepared 2% paraformaldehyde (Sigma-Aldrich, St Louis, Mo). FACS analysis was carried out with the use of a Becton-Dickinson Immunocytometry System and a FACS Calibur cytometer (Becton Dickinson, San Jose, Calif) with a minimum of 10,000 events counted. The following human antibodies were used: CD14-phycoerythrin, CD29FITC, CD40-FITC, CD44-FITC, CD80-PE, CD86-FITC, CD95-FITC, CD117-PE, CD152-PE, MHC class I–FITC, MHC class II–phycoerythrin (Becton-Dickinson), CD34-phycoerythrin, CD45-phycoerythrin (Miltenyi Biotec, Germany), CD90-phycoerythrin, CD105-phycoerythrin, and CD166-phycoerythrin (Serotec, Oxford, UK).

Osteogenic potential. We plated cells at a concentration of 1500 cells/cm^2 in the growth medium. Osteogenesis medium (Cambrex) containing 0.1 μmol/L dexamethasone, 0.05 mmol/L ascorbic acid-2-phosphate, 10 mmol/L β-glycerophosphate) was applied 24 hours after plating. The medium was refreshed every 3 to 4 days. Osteogenesis was assessed after on day 21 of culture. The expression of collagen type I was detected with the use of cytochemial staining. The cells were fixed in equal volumes of methanol and acetone for 1 minute at room temperature, washed with TBST (Dakocytomation, Kyoto, Japan), incubated with 3% hydrogen peroxide (Wako Pure Chemical Industries), and blocked with 10% normal rat serum at room temperature. Washed cells were incubated with mouse anti–human collagen type I monoclonal antibody (Sigma-Aldrich Japan, Tokyo, Japan) at a 1:50 dilution with the use of Dako antibody diluent (Dakocytomation) for 30 minutes at room temperature. Antimouse peroxidase-conjugated IgG (Sigma-Aldrich Japan) was used as secondary antibody at a 1:100 dilution, and 3-3′-diaminobenzidine in chromogen solution (Dakocytomation) was applied to the cells, which were counterstained with vector methyl-green nuclear countersolution (Vector Laboratories, Burlingame, Calif). We detected the expression of alkaline phosphatase by means of cytochemical staining with an alkaline phosphatase staining solution (0.1mg/mL Nafthol AS-MX phosphatase, 0.6mg/mL Fast-blue BB salt, 0.5% *N*-dimetyl-foramide, 2 mmol/L $MgCl_2$, 0.1 mol/L Tris-HCl; pH 8.8). A blue precipitate denoted a positive reacion. The in vitro mineralization was detected with the use of Alizarin red S (40 mmol/L, pH 4.2) staining after fixation in ice-cold ethanol (70%) for 1 hour.

Adipogenic potential. Cells were grown in adipogenic induction medium (Cambrex) containing h-insulin, L-glutamine, dexamethasone, indomethacin, and 3-isobuty-l-methyl-xanthine for 14 days. Adipocytes were visualized after fixation in formaldehyde buffer (4%) for 10 minutes followed by washing with isopropanol (3%). The cells were then stained with fresh oil red O (Sigma-Aldrich).

Production of lentiviral and adenoviral vectors. A lentivirus vector expressing GFP was produced by means of transient transfection into 293T cells in accordance with a calcium phosphate transfection protocol. We seeded 1×10^7 293T cells in 15-cm-diameter dishes and treated them with 0.01% poly-L-lysine (Wako) for 24 hours before transfection in DMEM (Invitrogen, Carlsbad, Calif) with 10% FBS (Invitrogen) and 75 mg/L kanamycin (Meji Seika, Tokyo, Japan) in a 5% CO_2 incubator at 37° C. We used 33.3 μg of plasmid DNA for the transfection in each of the dishes, which contained 15.3 μg of transfer vector plasmid pCS-CDF-CG-PRE (a gift from Dr Miyoshi, RIKEN; containing the GFP gene); 9 μg of packaging plasmid, pMDLg/p; 4.5 μg of Rev plasmid, pRSV-Rev; and 4.5 μg of envelope plasmid, pMD.G. To achieve precipitation, we used the following procedures. First we added the plasmids to a final volume of 3645 μL of sterilized water and 135 μL of 2.5 mol/L $CaCl_2$ and mixed them well. Next we added 1350 μL of 2×BBS, then mixed the DNA solution and incubated it for 20 minutes at room temperature. We resuspended the DNA solution by means of inversion and added it in drops to the culture dish, which we incubated in a 3% CO_2 incubator at 37° C. After 12 to 16 hours of incubation, the medium was replaced with 15 mL of DMEM containing 10 μmol/L forskolin (Wako), and the dish was then placed in a 5% CO_2 incubator at 37°C. The conditioned medium was collected after an additional 48 hours of incubation and filtrated through 0.45-μg cellulose acetate filters. The conditioned medium was ultracentrifuged twice, after which the virus pellet was resuspended in PBS and frozen at −80° C until it was needed for use in the experiment. The 293T cells were infected overnight in 6-well plates with serial dilutions of the conditioned medium from the 293T transient transfectants or with the concentrated viral stocks in the culture medium that was used for titration. The lentivirus titers were derived from the quantitative FACS (FACSort; Becton-Dickinson, San Jose, Calif) analysis performed with the 293T cells and expressed as IUs. Adeno-GFP was provided by the RIKEN BioResource Center.

Transduction of cells. MSCs (passage 2) grown in a flask for 1 week were detached with the use of trypsin-EDTA and replated in 6-well plates at a density of 5×10^4 cells in 1 mL of MSCGM per well. The medium was aspirated when the cells reached subconfluence. We added adeno-GFP and lenti-GFP diluted medium to the cells to achieve a multiplicity of infection of 20 (adeno-GFP) or 10 (lenti-GFP). After incubation at 37° C for 24 hours, we replaced the transduction medium with fresh MSCGM. We maintained the transduced MSCs by changing the medium every 3 days and replating the cells when they reached subconfluence. Cells were then analyzed for long-term expression of the transgene. The cells were kept for 5 weeks, with medium changes and passage before FACS was carried out.

RESULTS

Cell structure and proliferation. We cultured whole mononuclear fractions of UCB. Over the first 3 to 4 weeks, almost all of the stem cells died, leading to a very small viable cell population. The hematopoietic component of the culture survived for 4 to 6 weeks. The MSCs were identifiable as colonies of adherent cells with a fibroblastlike appearance, similar to those observed in bone marrow (Fig 1, *A* and *B*).

MSCs were replated at a density of 1000 cells/cm^2 by means of trypsinization when the cells reached 70% to 80% confluence. After repeated subcultures, the cultures contained a homogenous layer of fibroblastlike cells (Fig 1, *C* and *D*). These cells can be maintained in continuous culture for more than 6 months and 10 passages. Initially the growth rate was slow; it gradually increased between passages 2 and 7 and then decreased after passage 9, corresponding to 180 days of culture. We extrapolated a total expansion over 10 passages of 10^{11} cells (Fig 2).

Flow-cytometric characterization. We determined the immunophenotype of MSC to be monolayered single colony-derived adherent cells from UCB and compared

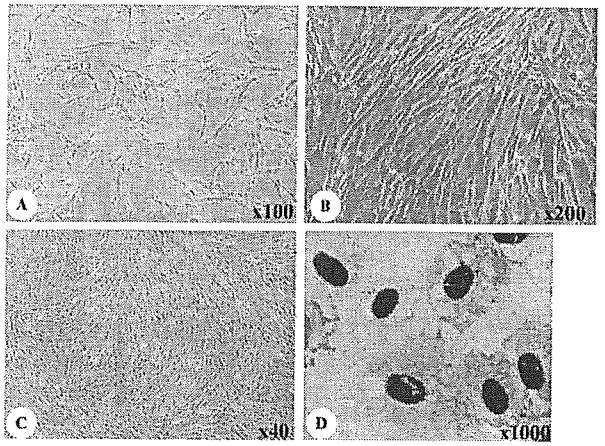

Fig 1. Structure of MSCs obtained from human UCB. Established, confluent MSCs in the culture displayed a typically homogeneous fibroblastlike pattern. (**A**) Phase-contrast view of MSCs cultured with MSCGM at passage 2, original magnification 100×. –; (**B**) same cells, original magnification 200×; (**C**) at day 60, as a confluent colony, original magnification 40×. (**D**) Cytospin of a trypsinized MSC colony stained with May-Giemsa stain. Data are representative of 3 independent experiments.

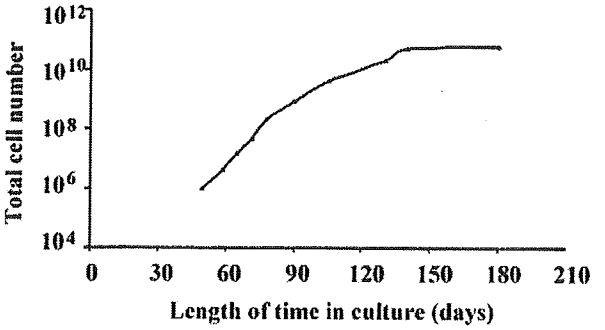

Fig 2. Growth curve of UCB-derived MSCs. Fifty days after we started the culture of UCB, the adherent fibroblast cells obtained from UCB reached subconfluence. We extrapolated the growth of MSCs from the number of cells counted during subculture of the cells (1000 cells/cm^2). Total extrapolated growth over time demonstrates different rates of growth during the 50 to 180 days after culture.

it with that of UCB-derived MNCs by means of flow cytometry. The MSCs were larger than lymphocytes, requiring significant adjustment of the flow cytometry gating established for lymphocytes (data not shown). The immunophenotypical profile of the MNC fraction changed significantly after the culture period, turning to typical MSC immunophenotypes that were positive for adhesion molecules, including β-1 integrin (CD29), hyaluronate receptor (CD44), Thy-1 (CD90), endoglin (CD105), and activated leukocyte cell adhesion molecule (CD166), as shown in Fig 3. Significantly, the MSCs were all CD45 negative, consistent with a nonhematopoietic origin and confirming that either hematopoietic or mononuclear cells had been depleted from the culture. In line with this finding, we detected no macrophages (CD14-positive cells) in the culture. Finally, the MSCs were all found to be negative for CD34 and stem cell–factor receptor (CD117). With respect to the markers known to participate strongly in immune activation, we found that MSCs were positive for MHC class I and Fas (CD95) but that they did not express MHC class II, one of the TNF receptor–superfamily members (CD40), B7-1 (CD80), B7-2 (CD86), cytotoxic lymphocyte–associated protein-4, or CTLA4 (CD152), as shown in Fig 3.

Osteoblstic differentiation potential of UCB-derived MSCs. In the presence of an osteogenic induction medium containing β-glycerophosphate, ascorbate, and dexamethasone, the UCB-derived MSCs exhibited clear changes in structure, from spindle-shaped to cuboidal, as they differentiated and mineralized. These cells stained positive for osteoblastic markers: collagen type I and alkaline phosphatase (Fig 4, *A* and *B*). When the confluent cells were incubated in osteogenic induction medium for 2 to 3 weeks, the UCB-derived MSCs formed a mineralized matrix in vitro, demonstrated by positive staining with Alizarin red S (Fig 4, *C*).

Adipogenic differentiation potential of UCB-derived MSCs. After 3 weeks of culture in the adipogenic induction medium containing h-insulin and dexamethasone, the UCB-derived MSCs formed adipocytes with lipid cytoplasm denoted by staining with oil red O (Fig 4, *D*).

Efficiency of gene transfer to UCB with the use of adenoviral and lentiviral vectors. We used efficient gene transfer involving adenoviral and lentiviral vectors containing the GFP gene for gene transfer into the primary UCB-derived MSCs. After infection with the adenoviral and lentiviral vectors, the MSC structure did not change. However, expression of the exogenous gene GFP was confirmed under fluorescence microscopy (Fig 5, *A–F*). We compared the efficiencies of expression of GFP 1, 3, and 5 weeks after infection by means of FACS analysis and analyzed the kinetics of gene expression of adeno-GFP and lenti-GFP. The percentage of adeno-GFP positive cells decreased noticeably after 1 week of infection. The percentage of GFP-positive cells infected with lenti-GFP was more than the percentage of adeno-GFP–positive cells after 5 weeks (Fig 6). The lentiviral vectors have a significant advantage over adenoviral vectors in the long-term stability of transgene expression in human UCB–derived MSCs.

DISCUSSION

Stem-cell transplantation represents a promising therapy for several degenerative and necrotic diseases.[4–7]

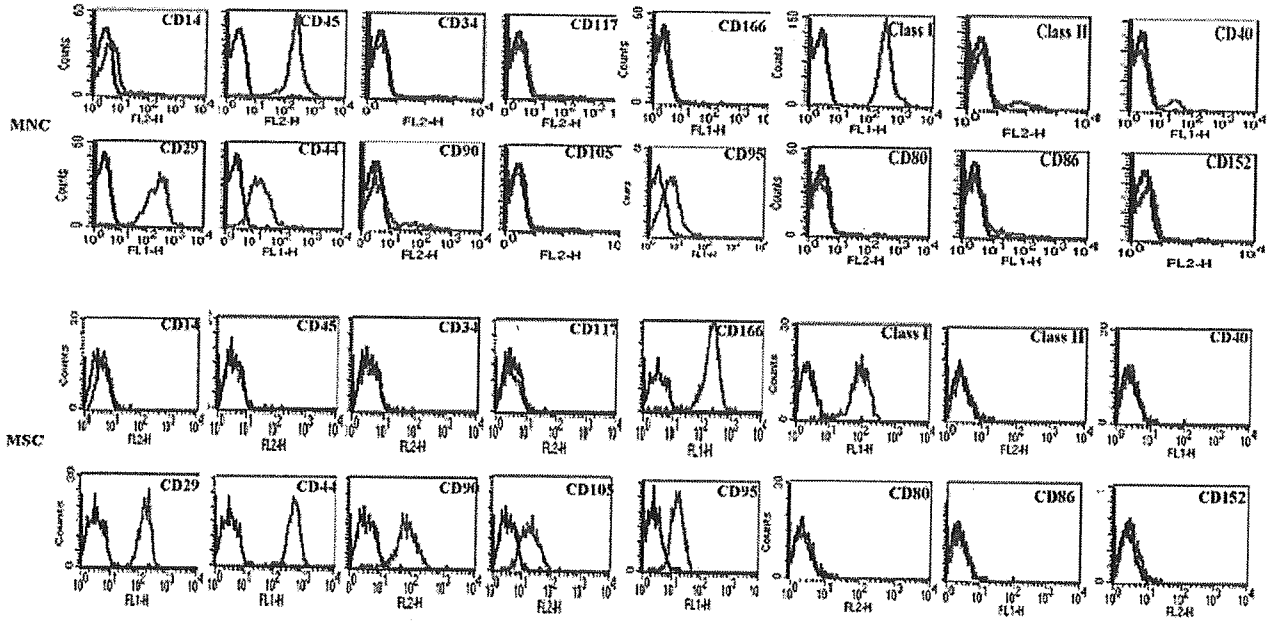

Fig 3. Immunophenotyping of MNC fraction and MSCs derived from UCB. Cells were labeled with FITC- or phycoerythrin-conjugated antibodies and examined by means of flow cytometory. Histograms demonstrating the expression of surface molecules were plotted against control (anti-IgG). The immunophenotypical profile of the MNC fraction changed significantly after 4 weeks of culture, to that of MSCs. MSCs expressed CD29, CD44, CD90, CD95, CD105, CD166, and MHC class I but not CD14, CD34, CD40, CD45, CD80, CD86, CD117, CD152, or MHC class II. Data are representative of 3 independent experiments.

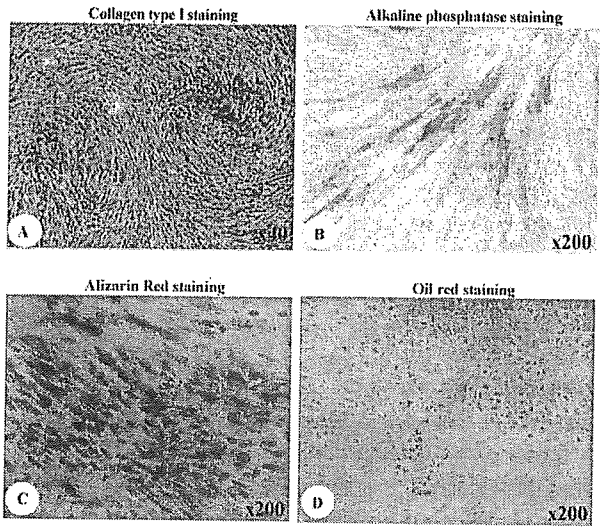

Fig 4. Expression of bone and fat phenotypes after exposure of MSCs to differentiation medium. MSCs were successfully differentiated along osteogenic and adipogenic lineages. Osteogenic differentiation was confirmed by means of (**A**) immunocytochemical staining for collagen type I (original magnification 40×), (**B**) cytochemical staining for alkaline phosphatase (original magnification 200×), and (**C**) the formation of a mineralized matrix stained with Alizarin red S (original magnification 200×). (**D**) Lipid-filled adipocyte detected with the use of oil red O staining (original magnification 200×). Data are representative of 3 independent experiments.

Many different types of stem cells reside in a range of tissue types. Among them, pluripotent stem cells have received a great deal of attention because of their capacity for multilineage differentiation. MSCs are fibroblastlike cells characterized by their capacity for rapid growth. They are also considered pluripotent stem cells.[20] MSCs are present in adult BM; they account for a small population but can be expanded exponentially under favorable conditions.[21,22] Some reports have also suggested that MSC may be effectively separated from many other tissues.[23–27]

Convenience of collection makes blood superior to other tissues as the source of therapeutic cells. In particular, UCB is considered as one of the best sources of therapeutic cells because the collection of these cells does not require invasive surgery. Hematopoietic stem cells are known to be present in UCB, but whether MSCs are also present in UCB remains a matter of dispute. Some reports have shown that UCB does not contain MSCs,[12,13,28–31] but the authors of many recent studies have reported that MSCs may be separated from UCB.[8,9,11,32,33] In addition, Lee et al[33] have demonstrated that immunophenotypes of clonally expanded cells derived from fresh UCB are similar to those of BM-derived MSCs. In spite of these reports, the presence of MSCs in UCB has yet to be unequivocally demonstrated.

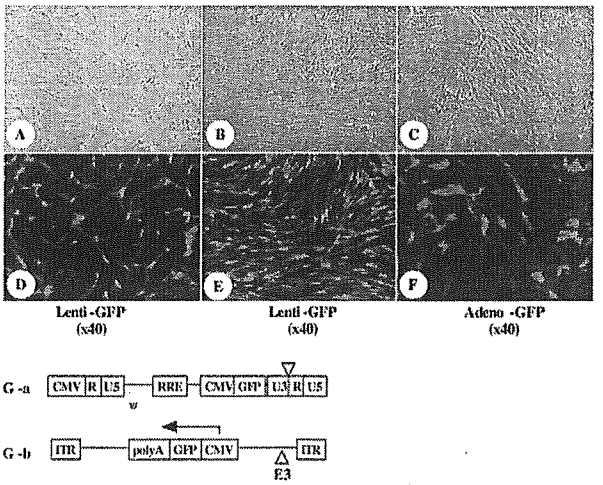

Fig 5. GFP transgene expression of MSC infected with adenoviral and lentiviral vectors. (**A**) Light photomicrograph and (**B**) fluorescence photomicrograph of MSCs cultured for 3 days after infection with lentiviral vector (original magnification 40×). (**C**) Light photomicrograph and (**D**) fluorescence photomicrograph of confluent MSCs cultured for 7 days after infection with lentivirus vectors (original magnification 40×). (**E**) Light photomicrograph and (**F**) fluorescence photomicrograph of confluent MSCs cultured for 7 days after infection with adenovirus vector (original magnification 40×). Data are representative of 3 independent experiments. (**G**) Construction of adenoviral and lentiviral vector. *G-a* = lenti-GFP; *G-b* = adeno-GFP; *CMV* = human cytomegalovirus immediate early promoter; *RRE* = Rev response element; *ITR* = inverted terminal repeat.

In this study, we showed that human UCB contains a small population of MSCs that are capable of differentiating into osteoblasts and adipocytes. These cells may be expanded and maintained in continuous culture for more than 6 months. As reported previously,[8,9,11,32,33] many similarities exist between MSCs isolated from UCB and BM. Furthermore, we were unable to grow hematopoietic colonies from UCB-derived MSCs in our culture system. However, we do not yet know the origin of these cells, so further studies are needed to understand whether they were derived from the same stem cells as the hematopoietic cells or had lost the ability to differentiate into hematopoietic cells as a result of the culture conditions used in this study.

As described previously,[34] the definition of MSCs is made difficult by the lack of a specific cell-surface marker that defines the progenitor population. In this study, we identified an immunophenotype of the MSCs. The results indicate the lack of hematopoietic marker expression (Fig 3), and UCB-derived MSCs are always CD34- and CD45-negative once cultures have been established. The expression of adhesion molecules was found to be similar in UCB- and BM-derived MSCs, with the exception of CD90 and CD166. In this study, the UCB-derived MSCs showed strong expression of CD90 and CD166, suggesting an abundance of osteoblast progenitors. These results differ from those of other researchers.[33] Our cells also expressed CD105 (endoglin, TGF-β receptor III). It is likely that TGF-β signaling plays a role in the control of chondrocyte differentiation from UCB-derived MSCs.

We also observed large interindividual variations in the ability of UCB to support the growth of UCB-derived MSCs. Similar observations have been reported by other researchers[33] and may support the existence of a true biologic variation among donors. More specific methods that identify UCB-derived MSCs and promote their attachment and growth are clearly needed.

Although we found UCB-derived MSCs to be capable of expressing antigens of multiple lineages in vitro, it will be important to demonstrate that these cells can function across lineage boundaries in vivo. Wide-ranging transplantation trials are therefore needed to further understand the capacity of these cells. Recent reports have shown that MSCs can engraft and differentiate when transplanted into experimental animals[35–37] and play a role in wound healing.[38–43] Furthermore, using a sheep-xenograft model, Liechty and colleagues successfully transplanted MSCs into fetal sheep.[44] Human MSCs have been engrafted and shown to persist in multiple tissues for as long as 13 months. These cells seem to have unique immunologic characteristics that permit persistence in a xenogenic environment. These properties suggest the potential usefulness of MSCs in cell- and gene-based therapies, as well in the treatment of a wide range of mesenchymal disorders.[45,46] MSCs have recently been investigated for their potential as platforms for the systemic delivery of therapeutic proteins in vivo after gene transfer.[17]

Although the authors of a variety of studies involving BM-derived MSCs and various viruses have attempted to transduce exogenous genes, no study involving UCB-derived MSCs has been reported until now. In this study we therefore focused the practice of gene transfer—in which a reliable gene-delivery system is required to transfer genes for use as platforms for the systemic delivery of therapeutic proteins—on UCB-derived MSCs. As a means of demonstrating the effectiveness of lentivirus vector in gene and cell therapy, we compared the efficiency of exogenous gene transduction and the kinetics of transduced gene expression to UCB-derived MSCs, using adenoviral and lentiviral vectors that are used in a wide variety of research, including cell- and animal-based studies and clinical tests against genetic and acquired disorders. The proportion of GFP-positive cells in the lenti-GFP group had a continuous-expression level of 83.0% at the end of 5 weeks. However, the proportion of GFP-positive

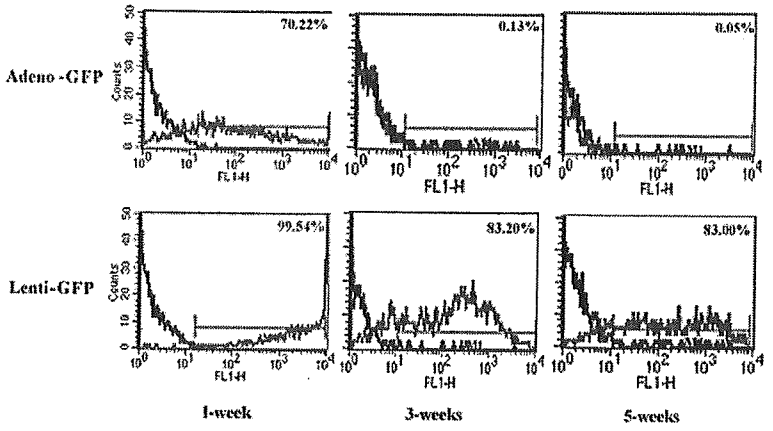

Fig 6. Kinetic representation of exogenous gene expression of MSCs transduced by adenoviral and lentiviral vectors. The efficiencies of gene transduction were compared after 1, 3, and 5 weeks by means of FACS analysis. We found the lentiviral vector more efficient than the adenovirus vector for transgene expression in human UCB-derived MSCs. Data are representative of 3 independent experiments.

cells in the adeno-GFP group declined rapidly, from 70% after 1 week to 0.05% after 5 weeks (Fig 6). These results indicate that the major advantage of lentiviral vectors is that they are capable of integrating their genomes into those of the host cells and therefore have the potential to enable long-term expression of the transgene. Lentiviral vectors have a significant advantage over adenoviral vectors with regard to the long-term stability of transgene expression in human UCB-derived MSCs, as described in BM-derived MSCs.[17] The differentiation status of cells after gene transfer is another important consideration. In this study, we found that the lentiviral vectors had no significant influence on the surface markers at the end of the 5-week experiment (data not shown).

The results of this study show that lentiviral vectors appear to be efficient in delivering and expressing transgenes in UCB-derived MSCs. One of the important clinical requirements of genetically modified MSCs is that they are stable and can provide long-term expression of the desired gene product, as well as regulation of gene expression according to the severity of the disease. The continuing development of lentiviral vectors may be an important advance in moving clinical gene transfer closer to the goal of being a viable option for the routine treatment of a variety diseases. Nevertheless, despite the challenges and questions that remain, lentiviral vectors do show promise for future clinical use.

In conclusion, we have shown that MSCs with high proliferation and differentiation potential are present in human UCB. Further, we have demonstrated for the first time that lentivirus vector can transduce exogenous gene and cause expression to persist. UCB should not be regarded as medical waste. On the basis of their great expansion capacity, as well as their differentiation potential, human UCB-derived MSCs should be regarded as attractive targets for cellular or gene-transfer therapeutic options.

We thank Dr. Hiromitsu Kimura for comments and useful suggestions.

REFERENCES

1. Mayani H, Lansdorp PM. Biology of human umbilical cord blood–derived hematopoietic stem/progenitor cells. Stem Cell 1998;16:153–65.
2. Koh LP, Chao NJ. Umbilical cord blood transplantation in adults using myeloablative and nonmyeloablative preparative regimens. Biol Blood Marrow Transplant 2004;10:1–22.
3. Huss R. Isolation of primary and immortalized CD34-hematopoietic and mesenchymal stem cells from various sources. Stem Cell 2000;18:1–9.
4. Horwitz EM, Prockop DJ, Fitzpatrick LA, Koo WW, Gordon PL, Neel M, et al. Transplantability and therapeutic effects of bone marrow–derived mesenchymal cells in children with osteogenesis imperfecta. Nat Med 1999;5:309–13.
5. McDonald JW, Liu XZ, Qu Y, Liu S, Mickey SK, Turetsky D, et al. Transplanted embryonic stem cells survive, differentiate and promote recovery in injured rat spinal cord. Nat Med 1999;5: 1410–2.
6. Orlic D, Kajstura J, Chimenti S, Jakoniuk I, Anderson SM, Li B, et al. Bone marrow cells regenerate infarcted myocardium. Nature 2001;410:701–5.
7. Pluchino S, Quattrini A, Brambilla E, Gritti A, Salani G, Dina G, et al. Injection of adult neurospheres induces recovery in a chronic model of multiple sclerosis. Nature 2003;422:688–94.
8. Erices A, Conget P, Minguell JJ. Mesenchymal progenitor cells in human umbilical cord blood. Br J Haematol 2000;109:235–42.
9. Goodwin HS, Bicknese AR, Chien SN, Bogucki BD, Quinn CO, Wall DA. Multilineage differentiation activity by cells isolated

from umbilical cord blood: expression of bone, fat, and neural markers. Biol Blood Marrow Transplant 2001;7:581–8.
10. Kakinuma S, Tanaka Y, Chinzei R, Watanabe M, Shimizu-Saito K, Hara Y, et al. Human umbilical cord blood as a source of transplantable hepatic progenitor cells. Stem Cells 2003;21:217–27.
11. Rosada C, Justesen J, Melsvik D, Ebbesen P, Kassem M. The human umbilical cord blood: a potential source for osteoblast progenitor cells. Calcif Tissue Int 2003;72:135–42.
12. Hows JM, Bradley BA, Marsh JC, Luft T, Coutinho L, Testa NG, et al. Growth of human umbilical-cord blood in longterm haemopoietic cultures. Lancet 1992;340:73–6.
13. Wexler SA, Donaldson C, Denning-Kendall P, Rice C, Bradley B, Hows JM. Adult bone marrow is a rich source of human mesenchymal "stem" cells but umbilical cord and mobilized adult blood are not. Br J Haematol 2003;121:368–74.
14. Satoh E, Osawa M, Tomiyasu K, Hirai H, Shimazaki C, Oda Y, et al. Efficient gene transduction by Epstein-Barr virus–based vectors coupled with cationic liposome and HVJ-liposome. Biochem Biophys Res Commun 1997;238:795–9.
15. Hamm A, Krott N, Breibach I, Blindt R, Bosserhoff A K. Efficient transfection method for primary cells. Tissue Eng 2002; 8:235–45.
16. Sakurai F, Mizuguchi H, Hayakawa T. Efficient gene transfer into human CD34+ cells by an adenovirus type 35 vector. Gene Ther 2003;10:1041–8.
17. Lee CI, Kohn DB, Ekert JE, Tarantal AF. Morphological analysis and lentiviral transduction of fetal monkey bone marrow–derived mesenchymal stem cells. Mol Ther 2004;9:112–23.
18. Ito H, Goater JJ, Tiyapatanaputi P, Rubery PT, O'Keefe RJ, Schwarz EM. Light-activated gene transduction of recombinant adeno-associated virus in human mesenchymal stem cells. Gene Ther 2004;11:34–41.
19. Brun AC, Fan X, Bjornsson JM, Humphries RK, Karlsson S. Enforced adenoviral vector–mediated expression of HOXB4 in human umbilical cord blood CD34+ cells promotes myeloid differentiation but not proliferation. Mol Ther 2003;8:618–28.
20. Jiang Y, Jahagirdar BN, Reinhardt RL, Schwartz RE, Keene CD, Ortiz-Gonzalez XR, et al. Pluripotency of mesenchymal stem cells derived from adult marrow. Nature 2002;418:41–9.
21. Prockop DJ. Marrow stromal cells as stem cells for nonhematopoietic tissues. Science 1997;276:71–4.
22. Pittenger MF, Mackay AM, Beck SC, Jaiswal RK, Douglas R, Mosca JD, et al. Multilineage potential of adult human mesenchymal stem cells. Science 1999;284:143–7.
23. Campagnoli C, Roberts IA, Kumar S, Bennett PR, Bellantuono I, Fisk NM. Identification of mesenchymal stem/progenitor cells in human first-trimester fetal blood, liver, and bone marrow. Blood 2001;98:2396–402.
24. Zuk PA, Zhu M, Mizuno H, Huang J, Futrell J W, Katz A J, et al. Multilineage cells from human adipose tissue: implications for cell-based therapies. Tissue Eng 2001;7:211–28.
25. Arai F, Ohneda O, Miyamoto T, Zhang X Q, Suda T. Mesenchymal stem cells in perichondrium express activated leukocyte cell adhesion molecule and participate in bone marrow formation. J Exp Med 2002;195:1549–63.
26. Sottile V, Halleux C, Bassilana F, Keller H, Seuwen K. Stem cell characteristics of human trabecular bone–derived cells. Bone 2002;30:699–704.
27. Romanov YA, Svintsitskaya VA, Smirnov VN. Searching for alternative sources of postnatal human mesenchymal stem cells: candidate MSC-like cells from umbilical cord. Stem Cell 2003; 21:105–10.
28. Mayani H, Gutierrez-Rodriguez M, Espinoza L, Lopez-Chalini E, Huerta-Zepeda A, Flores E, et al. Kinetics of hematopoiesis in Dexter-type long-term cultures established from human umbilical cord blood cells. Stem Cell 1998;16:127–35.
29. Gutierrez-Rodriguez M, Reyes-Maldonado E, Mayani H. Characterization of the adherent cells developed in Dexter-type long-term cultures from human umbilical cord blood. Stem Cells 2000;18:46–52.
30. Mareschi K, Biasin E, Piacibello W, Aglietta M, Madon E, Fagioli F. Isolation of human mesenchymal stem cells: bone marrow versus umbilical cord blood. Haematologica 2001;86:1099–100.
31. Yu M, Xiao Z, Shen L, Li L. Mid-trimester fetal blood–derived adherent cells share characteristics similar to mesenchymal stem cells but full-term umbilical cord blood does not. Br J Haematol 2004;124:666–75.
32. Lee MW, Choi J, Yang MS, Moon YJ, Park JS, Kim HC, et al. Mesenchymal stem cells from cryopreserved human umbilical cord blood. Biochem Biophys Res Commun 2004;320:273–8.
33. Lee OK, Kuo TK, Chen WM, Lee KD, Hsieh SL, Chen TH. Isolation of multipotent mesenchymal stem cells from umbilical cord blood. Blood 2004;103:1669–75.
34. Herzog EL, Chai L, Krause DS. Plasticity of marrow-derived stem cells. Blood 2003;102:3483–93.
35. Devine SM, Bartholomew AM, Mahmud N, Nelson M, Patil S, Hardy W, et al. Mesenchymal stem cells are capable of homing to the bone marrow of non-human primates following systemic infusion. Exp Hematol 2001;29:244–55.
36. Shake JG, Gruber PJ, Baumgartner WA, Senechal G, Meyers J, Redmond JM, et al. Mesenchymal stem cell implantation in a swine myocardial infarct model: engraftment and functional effects. Ann Thorac Surg 2002;73:1919–25; discussion 1926.
37. Toma C, Pittenger MF, Cahill KS, Byrne BJ, Kessler PD. Human mesenchymal stem cells differentiate to a cardiomyocyte phenotype in the adult murine heart. Circulation 2002;105:93–8.
38. Kinner B, Gerstenfeld LC, Einhorn TA, Spector M. Expression of smooth muscle actin in connective tissue cells participating in fracture healing in a murine model. Bone 2002;30:738–45.
39. Kinner B, Zaleskas JM, Spector M. Regulation of smooth muscle actin expression and contraction in adult human mesenchymal stem cells. Exp Cell Res 2002;278:72–83.
40. Skalli O, Pelte MF, Peclet MC, Gabbiani G, Gugliotta P, Bussolati G, et al. Alpha-smooth muscle actin, a differentiation marker of smooth muscle cells, is present in microfilamentous bundles of pericytes. J Histochem Cytochem 1989;37:315–21.
41. Mangeot PE, Duperrier K, Negre D, Boson B, Rigal D, Cosset FL, et al. High levels of transduction of human dendritic cells with optimized SIV vectors. Mol Ther 2002;5:283–90.
42. Eckes B, Colucci-Guyon E, Smola H, Nodder S, Babinet C, Krieg T, et al. Impaired wound healing in embryonic and adult mice lacking vimentin. J Cell Sci 2000;113:2455–62.
43. Zvaifler NJ, Marinova-Mutafchieva L, Adams G, Edwards CJ, Moss J, Burger JA, et al. Mesenchymal precursor cells in the blood of normal individuals. Arthritis Res 2000;2:477–88.
44. Liechty KW, MacKenzie TC, Shaaban AF, Radu A, Moseley AM, Deans R, et al. Human mesenchymal stem cells engraft and demonstrate site-specific differentiation after in utero transplantation in sheep. Nat Med 2000;6:1282–6.
45. Millington-Ward S, Allers C, Tuohy G, Conget P, Allen D, McMahon HP, et al. Validation in mesenchymal progenitor cells of a mutation-independent ex vivo approach to gene therapy for osteogenesis imperfecta. Hum Mol Genet 2002;11:2201–6.
46. Hutcheson KA, Atkins BZ, Hueman MT, Hopkins MB, Glower DD, Taylor DA. Comparison of benefits on myocardial performance of cellular cardiomyoplasty with skeletal myoblasts and fibroblasts. Cell Transplant 2000;9:359–68.

Available online at www.sciencedirect.com
SCIENCE DIRECT
Biochimica et Biophysica Acta 1725 (2005) 57 – 63
BIOCHIMICA ET BIOPHYSICA ACTA
BBA
http://www.elsevier.com/locate/bba

Membranous osteogenesis system modeled with KUSA-A1 mature osteoblasts

Satoshi Matsumoto[a,d], Isao Shibuya[a], Satoshi Kusakari[b], Kaoru Segawa[c], Taro Uyama[a], Akinori Shimada[d], Akihiro Umezawa[a,*]

[a]*Department of Reproductive Biology and Pathology, National Institute for Child Health and Development, 2-10-1 Okura, Setagaya-ku, Tokyo 157-8535, Japan*
[b]*Department of Pathology, Keio University School of Medicine, Tokyo 160-8582, Japan*
[c]*Department of Microbiology and Immunology, Keio University School of Medicine, Tokyo 160-8582, Japan*
[d]*Department of Veterinary Pathology, Tottori University, Tottori 680-8553, Japan*

Received 22 September 2004; received in revised form 16 May 2005; accepted 17 May 2005
Available online 17 June 2005

Abstract

Several stromal cells were established from murine bone marrow cultures. One of the KUSA subclones, KUSA-A1 cells, displays osteogenic characteristics in vitro and in vivo. The calcium deposition, osteocalcin release, and parathyroid hormone (PTH) responsiveness of KUSA-A1 cells indicate that they are mature osteoblasts or osteocytes. Bone had formed in subcutaneous tissue 1 week after subcutaneous injection of cells into immunodeficient mice. The osteogenesis by KUSA-A1 was not mediated by chondrogenesis and thus was considered to be membranous ossification. These unique characteristics of KUSA-A1 cells provide an opportunity to analyze the process of membranous ossification in detail.

Keywords: Membranous osteogenesis; Stromal cell; KUSA; Osteoblast; Gap junction

1. Introduction

The concept of regenerative medicine refers to the cell-mediated restoration of damaged or diseased tissue. Candidate cell sources for tissue regeneration include embryonic stem cells, fetal cells, and adult cells, such as marrow stromal cells [1], each of which has both advantages and drawbacks. Clinical trials with marrow stromal cells have been performed in patients with osteogenesis imperfecta [2] and osteoporosis [3,4], and marrow stromal cells are expected to be a good source of cell therapy [5]. Multipotent mesenchymal stem cells have been isolated from adult marrow and shown to differentiate into multiple cell types, such as osteoblasts, chondrocytes, adipocytes, myoblasts [1,5,6], cardiomyocytes [7,8], endothelial cells, and neuronal cells [9].

In the present study, we characterized a single cloned, immortalized stromal cell line, KUSA-A1, established from murine bone marrow cultures [6]. KUSA-A1 cells are capable of generating mature bone in vivo. They are a unique, mature osteoblast cell line and will serve as a very suitable model for in vivo osteogenesis.

2. Materials and methods

2.1. Cell culture

The stromal cell lines were isolated from long-term bone marrow cultures of C3H/He female mice and cultured as previously described [6,9–11]. Cells were cultured in Iscove's modified Dulbecco's medium (IMDM) supple-

* Corresponding author. Tel.: +81 3 5494 7047; fax: +81 3 5494 7048.
E-mail address: umezawa@1985.jukuin.keio.ac.jp (A. Umezawa).

0304-4165/$ - see front matter © 2005 Elsevier B.V. All rights reserved.
doi:10.1016/j.bbagen.2005.05.027

mented with 20% fetal bovine serum (FBS) and penicillin (100 μg/ml)/streptomycin (250 ng/ml) at 37 °C in humid air with 5% CO_2. Immortalized cells were obtained by frequent subculture for over a year. Cell lines from different dishes were subcloned by limiting dilution. The murine stromal cell lines are summarized in Fig. 1. In vitro calcification assay, osteocalcin production, and evaluation of parathyroid hormone (PTH) response were performed as previously described [10].

2.2. Measurement of alkaline phosphatase (ALP)

KUSA/A1 and MHCTC-E1 cells were analyzed by ALP assay as described [20].

2.3. Communication assay

Intercellular transfer Fluorescent Lucifer Yellow CH (Sigma, St. Louis, Missouri) was measured after the direct microinoculation of the dye into a KUSA-A1 cell as previously described [12,13].

2.4. RNA extraction and Northern blotting

RNA was prepared by homogenizing the specimens in guanidinium isothiocyanate, followed by centrifugation over a cesium chloride cushion as previously described [6,14]. The RNA was then electrophoresed in a 1.0% agarose gel, transferred to a nylon filter, and hybridized with a cDNA insert labeled with ^{32}P-dCTP by the random-primer method at 65 °C for 14–16 h in a buffer containing 5× SSPE (1× SSPE is 0.15 M NaCl, 10 mM NaH_2PO_4/Na_2HPO_4 (pH 7.4), and 1 mM EDTA), 5× Denhardt's solution (1× Denhardt's solution is 0.02% Ficoll polyvinylpyrrolidone and 0.02% BSA), 0.02% poly(A), and 1% SDS. The blots were washed with 2× SSC (1× SSC is 0.15 M NaCl and 0.015 M sodium citrate, pH 7.4) containing 1% SDS at room temperature and 65 °C. Final washing was performed with 0.1× SSC containing 0.1% SDS at 65 °C.

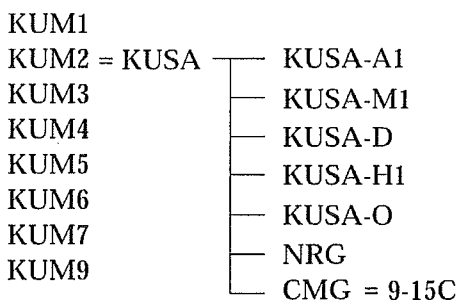

Fig. 1. The murine stromal cell lines. The clonal cells were designated KUM1 [6], KUM2/KUSA [6,9], KUM3-7 [6], and KUM9 [6,9]. The KUSA-A1 [6,11], KUSA-M1 [6], KUSA-D [6], KUSA-H1 [6], KUSA-O [6], and NRG [9] cells were subclones of KUSA cells. The CMG/9-15C cells are a subclone from KUSA cells that had been after exposed to 5-azacytidine [7,11]. The cell names are available at http://1985.jukuin.keio.ac.jp/umezawa/kum/kumh.html.

The blots were exposed to X-ray film at 80 °C with an intensifying screen. RNA blot analysis was carried out as previously described [6,14].

2.5. Transmission electron microscopy (TEM)

KUSA-A1 cells cultured in vitro for 14 days post-confluence were examined by TEM. The samples were fixed in 2.5% glutaraldehyde postfixed in 1% osmium tetroxide. They were rinsed in water, dehydrated, and embedded in epoxy resin. Ultrathin sections (70–90 nm) were cut and stained with 2% uranyl acetate and Reynold's lead citrate before being examined with a JEM-1200 EX microscope (JOEL Co., Japan) at 80 kV.

2.6. Inoculation of cells into mice

To determine the ability of KUSA, KUM3, KUM4, and NIH-3H3 cells to differentiate in vivo, freshly scraped KUSA-MTAg, KUM3-MTAg, KUM4-MTAg, and NIH3T3-MTAg cells (10^7 cells) were subcutaneously inoculated into Balb/c *nu/nu* mice (Sankyo Laboratory, Hamamatsu, Japan) as previously described [6]. Animals were sacrificed by cervical dislocation between 4 and 8 weeks after inoculation.

To determine the potential osteogenic activity of KUSA-A1 cells in vivo, freshly scraped KUSA-A1 cells (10^7 cells) were subcutaneously inoculated into severe combined immunodeficient (SCID) mice (Nippon CLEA, Hamamatsu, Japan). Subcutaneous specimens were resected between 1 and 4 weeks after inoculation and decalcified for a few days in formic acid. The implants were embedded in paraffin. Paraffin sections were deparaffinized, hydrated, and stained with hematoxylin and eosin.

All animals received human care incompliance with the "Principles of Laboratory Animal Care" formulated by the National Society for Medical Research, and the "Guide for the Care and Use of Laboratory Animals" prepared by the Institute of Laboratory Animal Resource and published by the US National Institute of Health (NIH Publication No. 86-23, revised in 1985). The operation protocols were accepted by the Laboratory Animal Care and the Use Committee of the National Research Institute for Child and Health Development, Tokyo, and Keio University School of Medicine.

3. Results

3.1. In vitro characterization of KUSA-A1 cells, single-cell-derived mature osteoblasts

In vitro, calcification by KUSA-A1 cells gradually increased during the culture period (Fig. 2A), and the amount of osteocalcin released into the culture medium also increased (Fig. 2B). The KUSA-A1 cells responded to PTH

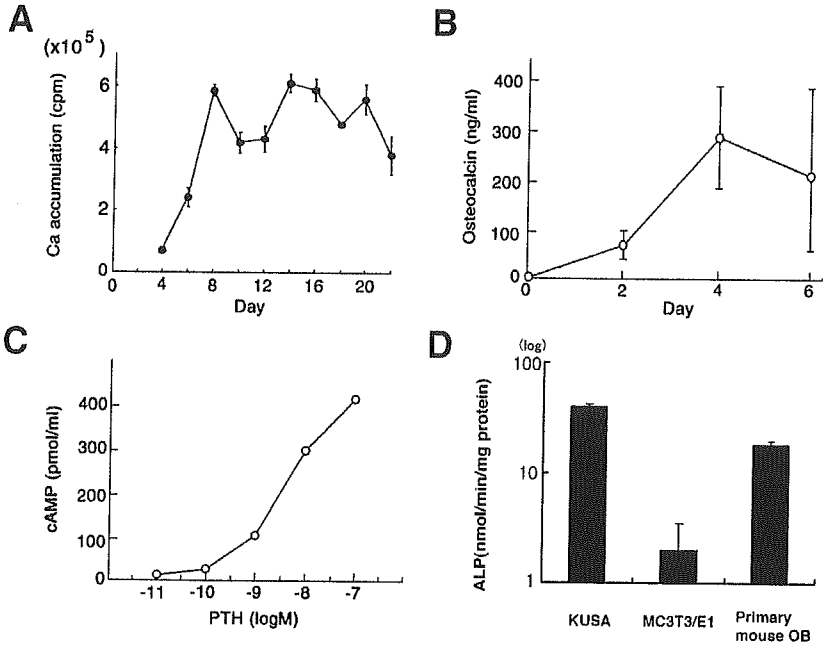

Fig. 2. Characteristics of KUSA-A1 cells as an osteoblast model. (A) Quantitative analysis of calcium deposition by KUSA-A1 cells. (B) Bone Gla protein (Osteocalcin) secretion by KUSA-A1 cells. (C) cAMP production after exposure to PTH. The KUSA-A1 cell response to PTH was assessed by measuring cAMP production. (D) ALP activity in KUSA-A1 cells and MC3T3-E1 cells at 7 days.

in a dose-dependent manner (Fig. 2C). The ALP activity of KUSA-A1 cells was approximately ten-fold higher than in MC3T3-E1 cells at 7 days (Fig. 2D). The calcium deposition and osteocalcin release indicated that KUSA-A1 cells are mature osteoblasts or osteocytes.

3.2. Morphology of KUSA-A1 cells: transmission electron microscopy (TEM) in vitro

Bone nodules [15] that had developed in KUSA-A1 cells cultured in medium supplemented with 10 mM beta-glycerophosphate were fixed and stained in situ by the von Kossa technique (Fig. 3A). The bone nodules consisted of an eosinophilic matrix containing ovoid cells resembling osteocytes, and the KUSA-A1 cells were arranged at the periphery of the nodule in the form of a periosteum-like cell layer. Mineral deposition by the KUSA-A1 cells demonstrated that they have the capacity to differentiate into osteoblasts, to deposit hydroxyapatite in well-developed bone matrix, and to express the differentiated state of osteoblasts.

Ultrastructurally, the matrix was electron-dense and was clearly produced by the cells in the bone nodules (Fig. 3B). The extracellular matrix produced by KUSA-A1 cells was

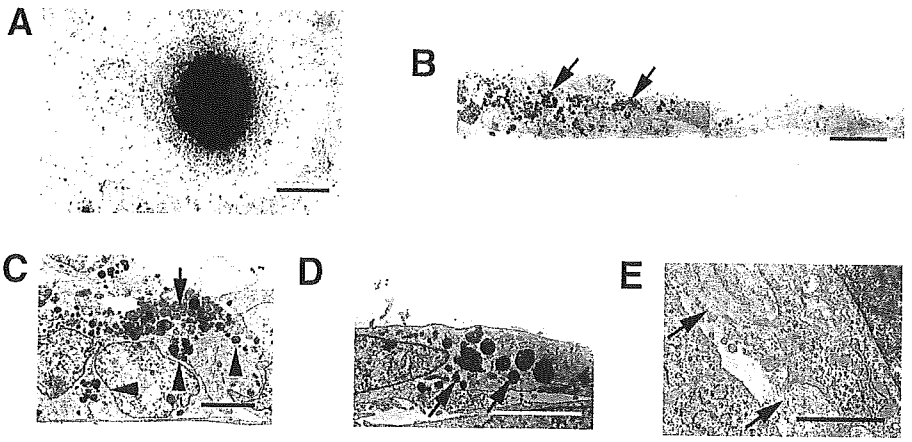

Fig. 3. Ultrastructural analysis of KUSA-A1 cells in culture. (A) KUSA-A1 cells 30 days after confluence. KUSA-A1 cultured in medium supplemented with beta-glycerophosphate was stained in situ by the von Kossa technique. Discrete mineralized nodules are seen. (B) Transmission electron micrograph (TEM) of a nodule present in a KUSA-A1 culture 14 days post-confluence. The extracellular matrix produced by KUSA-A1 cells was observed on the cell surface [arrow]. (C) High-power view of panel B. TEM revealed that the sphere of extracellular matrix produced by KUSA-A1 cells contained a small granular material [arrowhead]. (D) High-power view of a KUSA-A1 cell. Many lysosomal myelin-like figures [arrow] and rough endoplasmic reticulum are seen in its cytoplasm. (E) High-power view of KUSA-A1 cells. Abundant collagen fibrils are visible in the intercellular spaces [arrow], and the cytoplasm contains rough endoplasmic reticulum. Scale bars: 1 mm (A), 20 μm (B), 5 μm (C, D), and 1 μm (E).

observed on the cell surface (Fig. 3C). The cytoplasm of the spindle-shaped cells contained extensive, dilated, and rough endoplasmic reticulum and myelin-like lysosomes (Fig. 3D). Lysosome-rich cells were found in the bone nodules. These cells are probably similar to those observed in vivo [16] and in the primary bone cell cultures [17]. The cells produce abundant, orthogonally oriented collagen fibrils in the intercellular spaces (Fig. 3E), and these fibrils were also found in membrane folds.

3.3. Gap-junctional communication in KUSA-A1 cells

Gap-junctional communication is required for the osteoblast maturation process in culture [18,19], and we used the dye-transfer method to assess the gap-junctional communication between KUSA-A1 cells. When Fluorescent Lucifer Yellow CH was injected into a KUSA-A1 cell, the dye was rapidly transferred to the neighboring cells (Fig. 4A and B), implying that KUSA-A1 cells constitutively communicate with each other via gap junctions.

The expression of gap-junction genes by KUSA cells was investigated by blot hybridization of stromal cell RNA with a connexin 43 cDNA probe. H-1/A of the marrow preadipocyte cell line is a positive control. Distinct 3.0-kb mRNA bands were observed in all of the marrow stromal cell lines when tested with the connexin 43 cDNA probe (Fig. 4C), but no bands were detected in any of the cells when tested with a connexin 32 probe (data not shown).

3.4. Microscopic examination of large subcutaneous masses

NIH3T3, KUM3, KUM4, and KUSA cells transfected with MTAg were designated NIH3T3-MTAg, KUM3-MTAg, KUM4-MTAg, and KUSA-MTAg cells, respectively. Four weeks after subcutaneous inoculation of 10^7 NIH3T3-MTAg, KUM3-MTAg, KUM4-MTAg, KUSA-MTAg, and untransfected KUSA-A1 cells [6] into immunodeficient mice, masses had formed in the subcutaneous tissue. The masses were of three types histologically. Sarcoma-type masses were induced by NIH3T3-MTAg, KUM3-MTAg, and KUM4-MTAg cells and diagnosed as fibrocytic sarcoma; they did not contain bone. The tumors consisted of pleomorphic mesenchymal cells, including multinucleated bizarre giant cells (Fig. 5A and B). The second type of masses was sarcomas with complete bone formation. KUSA-MTAg cells induced sarcomas, most of which contained well-defined complete bone. These sarcomas exhibited an irregular woven pattern of pleomorphic spindle cells that included multinucleated tumor giant cells (Fig. 5C–E). The third type of masses consisted of complete bone and bone cavities with trilineage hematopoiesis. Untransfected KUSA cells formed bone (Fig. 5F–H). Untransfected KUSA-A1 cells, a subclone of the KUSA cells, also formed complete bone 4 weeks after inoculation (Fig. 5I and J). No sarcomatous cell proliferation was observed.

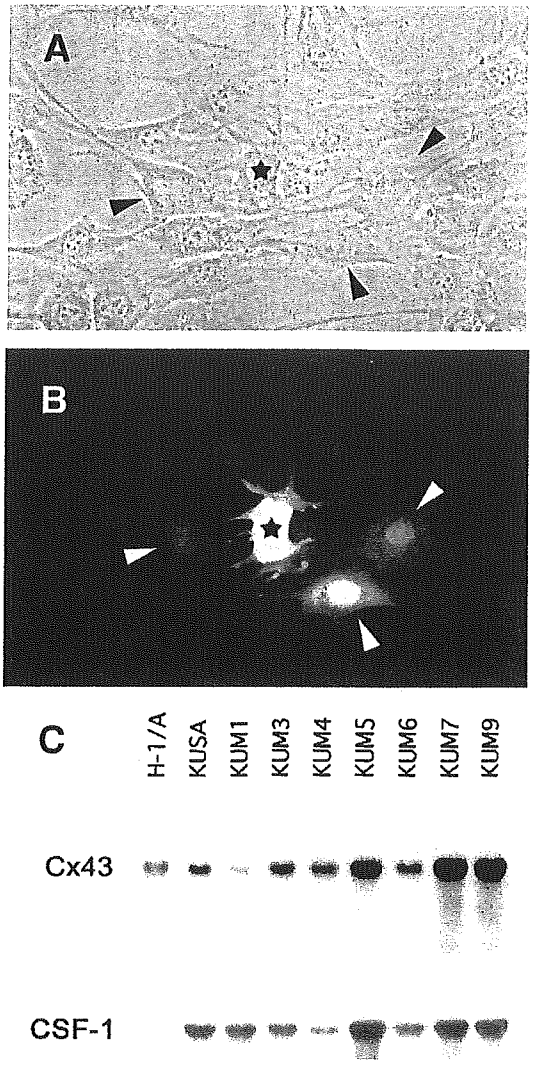

Fig. 4. Dye transfer in KUSA-A1 cells at semiconfluence. Intercellular communication was assessed by the dye transfer method. A and B: Phase-contrast micrograph (A) and fluorescence photograph (B) of KUSA-A1 cells. A KUSA-A1 cell [asterisk] was injected with Lucifer Yellow CH, and the dye was transferred to several adjacent cells. The dye has spread to three first-order-neighboring cells [arrowheads]. (C) Analysis of connexin 43 (Cx. 43) expression by KUSA, KUM1, KUM3, KUM4, KUM5, KUM6, KUM7, and KUM9 cells at semiconfluence. The same blot, which was rehybridized with the CSF-1, is shown for reference [6] in the lower panel.

3.5. Ossification by KUSA-A1 is membranous

To determine whether the ossification by KUSA-A1 is membranous or enchondral, we followed the time-course of KUSA-A1 ossification in the subcutaneous tissue of SCID mice after injecting cells 7 days post-confluence. The injected cells had produced a meshwork of collagen fibers and amorphous ground substance (osteoid matrix) at 1 week (Fig. 6A), and the fibers and ground substance markedly increased and became larger. The matrix was highly calcified at 4 weeks (Fig. 6B and C), and marrow cavities had formed inside the KUSA-A1 bone.